NESTED WELL PLASMA TRAPS

Darrell D. Dolliver, B.S.

Dissertation Prepared for the Degree of

DOCTOR OF PHILOSOPHY

UNIVERSITY OF NORTH TEXAS

August 2000

APPROVED:

Carlos A. Ordonez, Major Professor
Duncan Weathers, Committee Member
Jim Roberts, Committee Member
Zhibing Hu, Committee Member
Sam Matteson, Chair of the Department of Physics
C. Neal Tate, Dean of the Robert B. Toulouse School of Graduate Studies

Dolliver, Darrell, Nested Well Plasma Traps. Doctor of Philosophy (Physics), August 2000, 109 pp., 2 tables, 27 illustrations, bibliography, 48 titles.

Criteria for the confinement of plasmas consisting of a positive and negative component in Penning type traps with nested electric potential wells are presented. Computational techniques for the self-consistent calculation of potential and plasma density distributions are developed. Analyses are presented of the use of nested well Penning traps for several applications. The analyses include: calculations of timescales relevant to the applications, e.g. reaction, confinement and relaxation timescales, self-consistent computations, and consideration of other physical phenomenon important to the applications. Possible applications of a nested well penning trap include production of high charge state ions, studies of high charge state ions, and production of antihydrogen. In addition the properties of a modified Penning trap consisting of an electric potential well applied along a radial magnetic field are explored.

TABLE OF CONTENTS

LIST OF TABLES

LIST OF FIGURES

CHAPTER 1

NONNEUTRAL PLASMA CONFINEMENT IN SIMPLE PENNING TRAPS

In this chapter, a review of the confinement physics of nonneutral plasmas in Penning traps is presented. The nature of radial and axial confinement of nonneutral plasmas in such traps is explained, and the motions of particles in the trap are analyzed.

Penning traps have traditionally been used for the confinement of plasmas consisting of particles of a single sign charge as in pure electron or pure ionic plasmas. Although technically the term plasma refers to an ionized gas with overall neutrality, it has been applied to these nonneutral collections of charges because they share many features of neutral plasmas, e.g. Debye shielding. Debye shielding is characterized by a scale length λ_D. Macroscopic electric fields in a plasma do not normally exist over distances larger than λ_D in a direction parallel to a magnetic field. It should also be noted that the term plasma should only apply to a collection of charges if its Debye length λ_D is smaller than its spatial dimensions r_p so that the collection of charges is in the regime where collective effects are important. For simplicity the term plasma is used throughout this work regardless of the relative size of λ_D and r_p.

In its simplest form, a Penning trap consists of three cylindrical electrodes aligned end to end immersed in a constant axial magnetic field. Although other configurations are possible, as will be seen below, to assure radial confinement of the plasma, the configuration will need to be azimuthally symmetric. For the simple cylindrical

configuration, the center electrode is typically grounded while a positive voltage is applied to the end electrodes to confine a positive plasma (or a negative voltage is applied to confine a negative plasma).

Confinement of a plasma along the axis of this trap can be achieved simply by manipulating the voltage difference between the center and end electrodes. For a thermal plasma, as the change in potential energy a particle experiences as it leaves the central well region becomes much greater than its thermal energy, good axial confinement is ensured.

Radial confinement is achieved via the axial magnetic field. As presented elsewhere,[1] the effect of the magnetic field on the trapped particles can be seen by considering the total canonical angular momentum of the system

$$P_\theta = \sum_{i=1}^{N} m v_{\theta i} r_i + q A_\theta r_i$$

where N is the number of particles, and A_θ is the azimuthal component of the vector potential. For a low plasma density the vector potential is approximately equal to that which arises solely from the applied axial magnetic field, $A_\theta = Br/2$. For a large enough magnetic field the canonical angular momentum is dominated by the vector potential term

$$P_\theta \approx \frac{B}{2} \sum_{i=1}^{N} q_i r_i^2.$$

For a cylindrically symmetric system, P_θ is a constant of the motion. Thus, for a collection of like charged particles the mean squared radius of the particles is constant. Only a small fraction of the particles in such a collection can escape to a large radial position; the rest will always remain confined.

There are some additional issues with the radial confinement of a plasma within a Penning trap. The most important of these is the effect of neutral collisions.

Because the Penning trap contains an unneutralized plasma, a radial electric field necessarily exists inside the trap. The combined effect of the radial electric field and the axial magnetic field causes the charged particles of the plasma to undergo a net $\mathbf{E} \times \mathbf{B}$ rotation. Neutral particles present in the trap do not undergo this rotation, and the collisions between neutrals and the charged plasma column applies a torque which can alter the mean squared radius of the charged particles and allow the plasma to expand. This causes even a collection of like charged particles to have a finite confinement time.

An additional problem is field errors. Perfect azimuthal symmetry of the trap and magnetic field cannot be produced. This means that P_θ is, for any realizable trap, only approximately a constant of the motion. Expansion of the plasma and a finite confinement time also results. However, by minimizing field errors and maintaining a good vacuum to minimize the effect of neutrals, confinement times of several days have been achieved for pure nonneutral plasmas.

Rotation of a Nonneutral Plasma Column in a Penning Trap

The interior of an idealized Penning trap is filled with a uniform axial magnetic field. If no radial electric field exists, which will only occur in a neutral region, the orbit of particles would be along a helix with a radius equal to the Larmor radius, $r_L = mv_\perp/(|q|B)$, where $v_\perp$ is the velocity component perpendicular to the magnetic field.

However, within the region of the trap where an unneutralized plasma exists, there will necessarily be a radial electric field. The magnitude of the radial electric field for a single component plasma column of constant density n can be determined by applying Gauss' Law. The result is that for radial locations inside the radius of

a long plasma column $r < r_p$,

$$E_r = \frac{1}{2}\frac{rnq}{\epsilon_0}. \tag{1.1}$$

If we consider particles in this column to move along circular orbits centered on the trap axis, a balance must exist between the electric, magnetic and centrifugal forces. An expression of this balance takes the form

$$qv_\theta B = qE_r + \frac{mv_\theta^2}{r}$$

where v_θ is the particle's azimuthal velocity. Substituting the angular velocity, $\omega = v_\theta/r$, and the result for the electric field from Eq. (1.1) yields

$$\omega^2 - \frac{qB}{m}\omega + \frac{q^2 n}{2\epsilon_0 m} = 0.$$

This may be solved to give the two possible rotation frequencies for the plasma column[2]

$$\omega = \frac{qB}{2m} \pm \frac{qB}{2m}\sqrt{1 - \frac{2nm}{B^2\epsilon_0}}.$$

This may be written in terms of the cyclotron frequency, $\omega_c = qB/m$, and plasma frequency, $\omega_p = \sqrt{nq^2/(\epsilon_0 m)}$, yielding

$$\omega = \frac{\omega_c}{2}(1 \pm \sqrt{1 - \frac{2\omega_p^2}{\omega_c^2}}). \tag{1.2}$$

Because it necessarily creates a radial electric field, a nonneutral plasma column in a Penning trap rotates. A neutral plasma column will not undergo this rotation.

Single Particle Orbits

Moving away from the assumption that each particle travels on a circular orbit centered on the trap axis, we may examine the motion of individual particles of

the plasma. The force on a particle is $\mathbf{F} = q(\mathbf{E} + \mathbf{v} \times \mathbf{B})$ where $\mathbf{B} = B_0\hat{\mathbf{z}}$, and $\mathbf{E} = rnq/(2\epsilon_0)\hat{r}$ if we are far away from the confining electrodes.

In this region, the axial force on a particle is zero. Switching to Cartesian coordinates and evaluating the other force components we may write

$$\begin{aligned} m\ddot{x} &= \frac{nq}{2\epsilon_0}x + qB_0\dot{y} \\ m\ddot{y} &= \frac{nq}{2\epsilon_0}y - qB_0\dot{x}. \end{aligned}$$

These equations may be rewritten in terms of the cyclotron and plasma frequencies

$$\ddot{x} = \frac{\omega_p^2}{2}x + \omega_c\dot{y} \tag{1.3}$$

$$\ddot{y} = \frac{\omega_p^2}{2}y - \omega_c\dot{x}. \tag{1.4}$$

The analysis will be greatly simplified by making a transformation to a frame with new variables (x', y') which rotates at the average plasma rotation frequency ω

$$\begin{aligned} x' &= x\cos\omega t - y\sin\omega t \\ y' &= y\cos\omega t + x\sin\omega t. \end{aligned}$$

After making this substitution Eqs. (1.3) and (1.4) become

$$\begin{aligned} \ddot{x'} &= \dot{y'}(-2\omega + \omega_c) + x'(\omega^2 + \frac{\omega_p^2}{2} - \omega_c\omega) \\ \ddot{y'} &= \dot{x'}(2\omega - \omega_c) + y'(\omega^2 + \frac{\omega_p^2}{2} - \omega_c\omega) \end{aligned}$$

However, from Eq. (1.2) we see that $\omega^2 + \frac{\omega_p^2}{2} - \omega_c\omega$ is zero. Thus, in the rotating frame the equations of motion are

$$\ddot{x'} = \dot{y'}(-2\omega + \omega_c) \tag{1.5}$$

$$\ddot{y'} = \dot{x'}(2\omega - \omega_c). \tag{1.6}$$

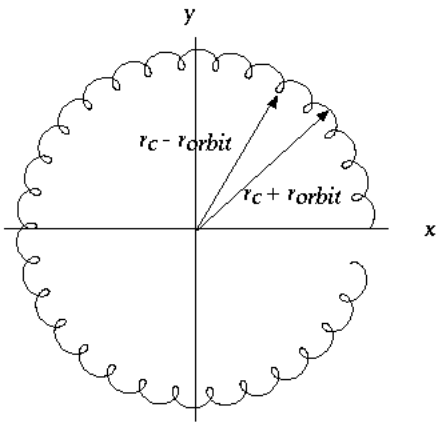

FIG. 1.1. The trajectory of a particle in a Penning trap containing a completely nonneutralized plasma.

Consequently, in the frame of reference which rotates with the plasma column, the motion of a particle is circular with period $T = 2\pi/(2\omega - \omega_c)$. An example of the particle orbit in the laboratory frame is shown in Fig. 1.1.

The solution of Eqs. (1.5-1.6) can be written

$$x' = x'_0 - \frac{v'_{y0}}{\omega'} + \frac{v'_{y0}}{\omega'}\cos(\omega' t) + \frac{v'_{x0}}{\omega'}\sin(\omega' t) \tag{1.7}$$

$$y' = y'_0 + \frac{v'_{x0}}{\omega'} + \frac{v'_{y0}}{\omega'}\sin(\omega' t) - \frac{v'_{x0}}{\omega'}\cos(\omega' t) \tag{1.8}$$

where (x'_0, y'_0) is the initial location of the particle in the rotating frame of reference, (v'_{x0}, v'_{y0}) is the initial velocity, and $\omega' = 2\omega - \omega_c = \pm q/m\sqrt{(}B^2 - (2nm)/\epsilon_0)$. In the rotating frame the circular orbits have a radius $r_{orbit} = v_\perp/\omega' = v_\perp/(\pm q/m\sqrt{(}B^2 - (2nm)/\epsilon_0)$. In the laboratory frame the radial position of the particle varies from $r = r_c - r_{orbit}$ to $r = r_c + r_{orbit}$, where r_c is the radial location of the particle's guiding center. This illustrates the nature of magnetic confinement. As B becomes large, r_{orbit} becomes small, and the particles never move far from $r = r_c$.

When $2\omega = \omega_c$, $\omega' = 0$ and the solution to Eqs. (1.5-1.6) becomes straight lines in the rotating reference frame. Substituting in the definitions of ω_c and ω we find that this occurs when $n = \frac{\epsilon_0 B^2}{2m}$. This is known as the Brillouin density limit, and confinement of a nonneutral plasma at a density greater than this in a Penning trap with an axial magnetic field is not possible.

REFERENCES

[1]T. M. O'Neil, "Plasmas with a single sign of charge," in *Non-Neutral Plasma Physics*(American Institute of Physics.

[2]R. C. Davidson, *Physics of Nonneutral Plasmas*, Addison-Wesley Publishing Company, Redwood City, California, 1990.

CHAPTER 2

CONFINEMENT OF PLASMAS WITH A NEUTRAL OR PARTIALLY NEUTRALIZED REGION IN NESTED WELL PENNING TRAPS

Malmberg/Penning plasma traps (i.e., Penning traps that employ cylindrical electrodes) have long been used to confine plasmas consisting of particles that have a single sign of charge.[1] Traps of this type often consist of three cylindrical electrodes that are aligned end to end along the axis of the trap. As described in Chapter 1, this series of electrodes creates a static potential well capable of confining the plasma axially. Radial confinement is achieved by placing the electrodes in a solenoidal magnetic field.

Another possibility is the use of Malmberg/Penning traps with nested electric potential wells for confining two overlapping plasma components with opposite sign charge.[2–4] In the present chapter different scenarios which may result in confinement of two oppositely charged plasma components with overlap are presented. A numerical method which is used for self-consistently calculating the potential and charge distributions is detailed. Methods for calculating other properties of nested well traps are analyzed.

Confinement of Two Oppositely Signed Plasmas with a Region of Overlap

To create a trap suitable for confining two oppositely charged plasmas the series of electrodes illustrated in Fig. 2.1 is considered. For simplicity, it is assumed that the positive plasma species is confined in the inner well and the negative species is confined in the outer well, although the sign of the electrode potential may be

reversed and the role of the plasmas switched.

The nested well trap is composed of a series of five hollow cylindrical electrodes with inner radius r_w centered upon the z axis of the trap which are used to create a nested well potential profile. The center electrode is of length L_0 and is typically held at zero volts. The pair of electrodes to either side of the center electrode, hereafter referred to as the inner electrodes, are of length L_1 and are held at voltage V_1. The outer set of electrodes are of length L_2 and are held at voltage V_2. The entire set of electrodes is placed in a constant axial magnetic field. By careful choice of the values for V_1 and V_2 and other parameters it is possible to create a situation wherein the potential step caused by the inner electrodes will keep a positively charged plasma adequately confined axially in the region of the central electrode while a negatively charged plasma is similarly confined by the outer electrodes with a significant degree of overlap of the positive plasma.

Criteria for Confinement with Overlap

For a plasma at thermal equilibrium in an electric potential well, a criterion for good confinement may be expressed as $q\Delta\phi_w/T \gg 1$ where $\Delta\phi_w$ is the depth of the electric potential well, q is the magnitude of the charge on a particle of the plasma, and T is the temperature of the plasma in energy units. Within the nested well the criterion for having the outer well species overlap the inner well species significantly is $q\Delta\phi_{iw}/T \lesssim 1$ where $\Delta\phi_{iw}$ is the depth of the inner well. To achieve overlap between plasma components, the thermal energy of the particles confined by the outer well must be at least comparable to the change in its potential energy between the inner and outer well. To achieve good confinement of a plasma, the change in its potential energy to leave the well must be much larger than its thermal

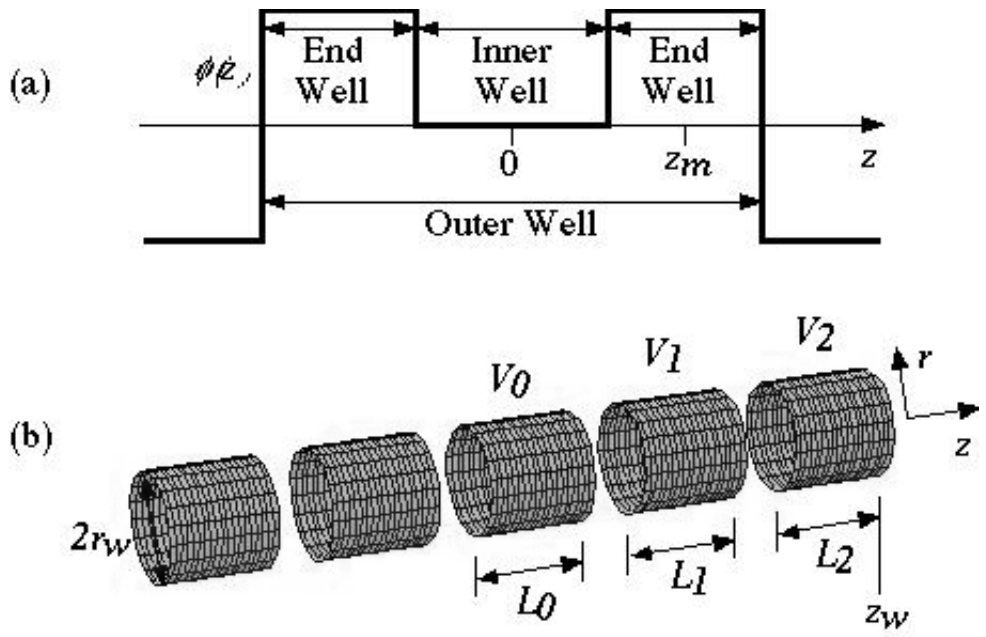

FIG. 2.1. (a) The applied electrode potential for a nested well plasma trap. (b) The electrode configuration required to produce the nested well potential illustrating various trap parameters.

energy.

There are several situations in which the confinement criteria for both the inner well and outer well plasma species can be satisfied simultaneously with the condition for overlap between the plasma species.[4] For two equal but opposite charge state thermal plasmas, e.g., a hydrogen plasma, this is possible only if the temperature of the inner well component is significantly smaller than the temperature of the outer well component. For a plasma consisting of two equal temperature Maxwellian components, confinement of both species with a significant degree of overlap is only possible if the inner well species has a higher charge state than the outer well species. Additionally, it is possible to confine equal charge state, equal temperature plasma components with a region of overlap if one of those plasma components is in a nonequilibrium state.

For the nonequilibrium approach, a suitable plasma state can be created by allowing a plasma at equilibrium to flow into an initially empty well[5–7]. The plasma will move through the regions of low potential energy quickly and will consequently have a lower density there than in some regions of higher potential energy. This is known as an "antishielding" state because a plasma in this state will tend to exaggerate the depth of a potential well instead of diminishing or "shielding" it as an equilibrium plasma state would. Because one plasma component is in a nonequilibrium state there will be a relaxation to a Maxwellian distribution due to collisions or microinstabilities, and the components will separate. It will be necessary to use a time-dependent potential to re-establish the nonequilibrium distribution.

Of the three possible methods for achieving confinement with overlap, the only direct experimental evidence available appears to have established that the simulta-

neous confinement of two overlapping equal magnitude opposite charge plasmas with disparate temperatures is possible.[2] These experimental results have shown simultaneous confinement of electrons and hotter protons within a nested well. Overlap was achieved such that sympathetic cooling occurred between the two species. These results do not appear to show the existence of a neutral overlap region, but theoretically it should be possible to confine even a plasma with a neutral region using a solenoidal magnetic field and axial electric field.

Confinement with overlap is possible in the case of plasma components with disparate charge states using static electric potential wells. The use of a two-temperature approach will require a time-dependent alteration of electrode voltages to counteract the temperature equilibrating effect of interparticle collisions. The use of a nonequilibrium distribution will require a time dependent voltage to counteract the distribution's relaxation to equilibrium through collisions or microinstabilities.

Computational Methods

A two dimensional self-consistent calculation of the electric potential and particle distributions is now described. For the purposes of this computation, gaps between the electrodes are neglected to allow for quicker numerical computation, or alternately, one may assume the size of the gaps between electrodes are smaller than the computational grid size. This is a commonly used approximation for numerical computation of plasma properties.[8–11] An actual experimental setup would likely feature larger gaps between electrodes. Additionally, for computational ease the open electrode configuration is capped at both ends by a circular electrode of voltage V_2. This computational model should give results applicable to an open ended trap having $L_2 \gg r_w$.

Two dimensional self-consistent calculations of the electric potential and particle distributions within a nested well trap were performed for several different sets of parameters via a finite difference numerical method.[8] The results generated are useful in determining what trap parameters are required to create a suitable well depth and plasma overlap. This method is used to demonstrate sets of parameters which result in a well confined plasma for various applications, typically with a neutral overlap region.

The particular finite difference method used is a sequential-over-relaxation (SOR) method. Its derivation follows. Due to the geometry of the traps it will be convenient to begin with Poisson's equation in cylindrical coordinates. With azimuthal symmetry assumed, Poisson's equation is

$$\frac{\partial^2\phi}{\partial r^2} + \frac{1}{r}\frac{\partial\phi}{\partial r} + \frac{\partial^2\phi}{\partial z^2} = f(r,z)$$

where $f(r,z) = -\rho(r,z)/\epsilon_0$. The particular ρ which is used is discussed in the section below. An analogous finite difference equation for a lattice is obtained by making the following replacements:

$$\begin{aligned}
\frac{\partial^2\phi}{\partial r^2} &\rightarrow \frac{\phi_{i+1,j} - 2\phi_{i,j} + \phi_{i-1,j}}{\Delta r^2} \\
\frac{\partial\phi}{\partial r} &\rightarrow \frac{\phi_{i+1,j} - \phi_{i-1,j}}{2\Delta r} \\
\frac{\partial^2\phi}{\partial z^2} &\rightarrow \frac{\phi_{i,j+1} - 2\phi_{i,j} + \phi_{i,j-1}}{\Delta z^2} \\
f(r,z) &\rightarrow f_{i,j} \\
r &\rightarrow r_i = \Delta r(i-1)
\end{aligned}$$

where Δr and Δz are the grid sizes, and i and j are the grid indices for the r and z axes respectively. This particular finite difference scheme is spatially centered. It

should be noted that it is necessary for accuracy to choose the grid spacings Δr and Δz on the order of one half the Debye length or smaller.[8] The computational region and grid variables are demonstrated in Fig. 2.2.

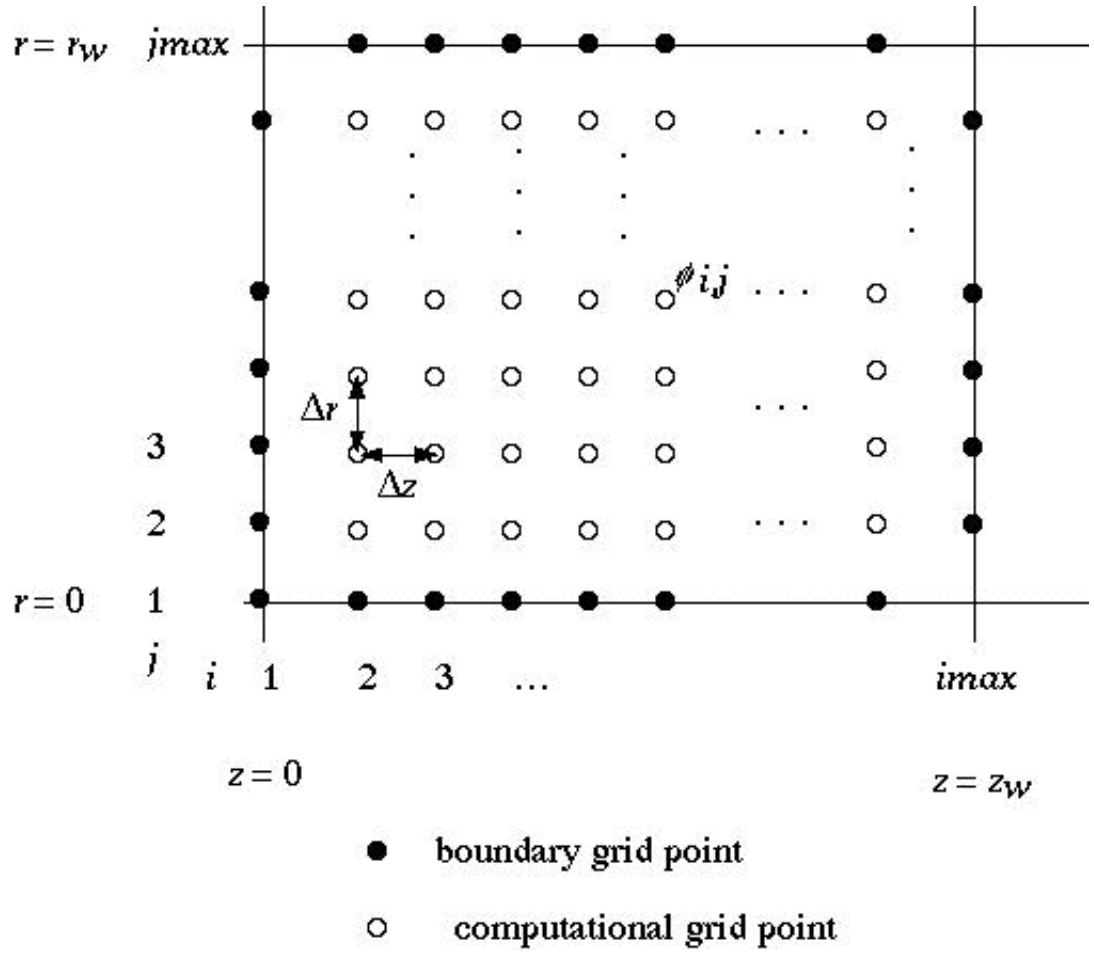

FIG. 2.2. The computation area and grid variables used in the SOR calculation of electric potential.

The resulting simple relaxation method algorithm is obtained when the finite difference version of Poisson's equation is solved for $\phi_{i,j}$,

$$\phi_{i,j}^{n+1} = -\frac{\Delta z^2 \Delta r^2}{2(\Delta z^2 + \Delta r^2)} \left[\frac{\left(1 + \frac{\Delta r}{2r_i}\right)\phi_{i+1,j}^n + \left(1 - \frac{\Delta r}{2r_i}\right)\phi_{i-1,j}^n}{\Delta r^2} + \frac{\phi_{i,j+1}^n + \phi_{i,j-1}^n}{\Delta z^2} - f_{i,j} \right].$$

The superscript of ϕ refers to the computational time step. The algorithm is changed from simultaneous to sequential by doing the averaging "in place." As soon as ϕ is calculated for one grid point , the new value is used in all proceeding calculations in that time step. In other words, if the program begins calculating at grid point $(i, j) = (1, 1)$ and proceeds to loop over i and j the previous equation could be rewritten as

$$\phi_{i,j}^{n+1} = -\frac{\Delta z^2 \Delta r^2}{2(\Delta z^2 + \Delta r^2)} \left[\frac{\left(1 + \frac{\Delta r}{2r_i}\right) \phi_{i+1,j}^{n} + \left(1 - \frac{\Delta r}{2r_i}\right) \phi_{i-1,j}^{n+1}}{\Delta r^2} + \frac{\phi_{i,j+1}^{n} + \phi_{i,j-1}^{n+1}}{\Delta z^2} - f_{i,j} \right],$$

so that the new values for ϕ are used as soon as they become available. This can speed up convergence over the first few time steps and is easy to implement as it obviates the need to store both an old and new value for $\phi_{i,j}$.

A further improvement to the convergence can be made by changing from a simple relaxation to an over-relaxation algorithm. This algorithm over corrects for ϕ at each time step in the following way,

$$\phi_{(SOR)i,j}^{n+1} = \omega \phi_{i,j}^{n+1} + (1 - \omega) \phi_{i,j}^{n} \tag{2.1}$$

where $\phi_{i,j}^{n+1}$ is the result for ϕ given by the sequential simple relaxation algorithm, and ω is the "acceleration" factor, a number between 1 and 2. The optimal value for ω is given by[12]

$$\omega = \frac{2}{1 + \sqrt{1 - \chi^2}}$$

where

$$\chi = \frac{\Delta z^2 \cos(\pi / i_{\max}) + \Delta r^2 \cos(\pi / j_{\max})}{\Delta z^2 + \Delta r^2}.$$

Boundary conditions are implemented by surrounding the computational grid with a series of boundary grid points. The boundary points either carry a fixed

potential or are updated to equal the value of the potential of the nearest computational grid point in the z or r direction after each computational step. This implements a Dirichlet or Neumann boundary condition respectively. See Appendix A for a discussion of alternate methods of setting boundary conditions and the effect on the accuracy of the solution. The boundary potential values are used in the calculation of neighboring computational grid points. An example of the SOR code used in the following chapters is presented in Appendix B.

The SOR method is typically marked by a lack of convergence for many computational timesteps followed by a rapid convergence. Testing for convergence can be done many ways. A common convergence test is to sum up over all grid points the square of the difference between the value of ϕ at the current and previous time step. This sum is known as the residual. The code may be iterated until the residual per grid point reaches a specified accuracy goal.

Derivation of Plasma Density Distributions within the Nested Well

To implement the SOR calculation of the trap potential requires the charge density ρ. A charge density could be fixed, or a self consistent determination of the particle density distributions within the trap could be carried out for each plasma species. Several possible assumptions can be made about the density distribution of a plasma species.

Local Thermal Equilibrium Density Distribution

A situation in which a plasma component obeys a Maxwell-Boltzmann distribution along each magnetic field line is known as local thermal equilibrium. This should not be confused with the local thermal equilibrium charge state distribution, which is an equilibrium between three body recombination and collisional ionization.

If local thermal equilibrium may be assumed, then a radial profile may be specified for the plasma, and the density distribution takes the form[4]

$$n(r,\phi) = -\frac{n_0}{\epsilon_0} h(r) \exp\left(-\frac{q}{kT}(\phi(r,z) - \phi(r,0))\right)$$

where $h(r)$ is the specified radial profile which is defined to have a value of 1 at the origin of the trap. The form $h(r) = 1 - (r/r_w)^\alpha$ where $\alpha = -2.3/\ln(1 - \lambda_D/r_w)$ may be used to give the plasma a radial profile which is radially flat until within about one Debye length of the wall where it decreases rapidly to zero.[4] In general this expression for n will be used for computational ease.

Cut-off Maxwellian Density Distribution

A further alternative is to assume a cutoff Maxwellian distribution which will exclude particles that will leave the trap in the r or z direction. Breaking down the distribution function $f(\mathbf{r}, \mathbf{v})$ into a part dependent on v_z , denoted f_z, and a part dependent on $v_\perp$, denoted $f_\perp$, we can include step functions to remove any particles which would not be confined in the well. The distribution of velocities parallel to z becomes

$$f_z(r,z,v_z) = C_1 \exp\left(-\beta v_z^2 - \psi(r,z)\right) \Theta\left(v_{z\max} - |v_z|\right).$$

Here C_1 is a normalization factor, $\beta = m/(2T)$, $v_{z\max} = \sqrt{(\psi_m(r) - \psi(r,z))/\beta}$, $\psi = Ze\phi(r,z)/T$, and $\psi_m(r)$ is the maximum value of the normalized potential energy which occurs along a magnetic field line at r.

In a similar way, the distribution of velocities in the directions perpendicular to z is given a cutoff. Assuming the plasma component is in a neutral region, and therefore the particle motion is about a helix with radius equal to the Larmor radius, $r_L = \frac{mv_\perp}{qB}$,

$$f_\perp(r_c, v_\perp) = C_2 v_\perp e^{-\beta v_\perp^2} \Theta\left(v_{\perp\max} - v_\perp\right) \tag{2.2}$$

where $v_{\perp\max} = qB(r_w - r_c)/m$, B is the magnetic field, r_c is the radial location of the center of the particle's gyro-orbit. This removes from the distribution those particles whose gyro-orbits intersect the electrode walls.

For particles which have a small Larmor (cyclotron) radius the assumption may be made that $r_c \approx r$. Using this assumption, the particle distribution function $f = f_\perp(r, v_\perp) f_z(r, z, v_z)$ may be integrated over velocity space to obtain a particle density distribution

$$\begin{aligned} n(r,z) &= \int_{-\infty}^{\infty}\int_{0}^{\infty} f_z(r,z,v_z) f_\perp(r,v_\perp) dv_\perp dv_z \\ &= \frac{n_0 \mathrm{e}^{-\psi(r,z)+\psi(0,0)}\left(1-\mathrm{e}^{-\beta(qB(r-r_w)/2)^2}\right)}{\left(1-\mathrm{e}^{-\beta(qBr_w/2)^2}\right)} \\ &\quad \times \frac{\operatorname{erfc}\left(\psi_m(r)-\psi(r,z)\right)\Theta(z_m-z)}{\operatorname{erfc}(\psi_m(0)-\psi(0,0))}. \end{aligned} \tag{2.3}$$

Antishielding Density Distribution

If a plasma is initially confined in a square potential well at a potential ϕ_{ext} with a Maxwellian distribution and density n then allowed to flow into a well with a potential of $\phi(x)$, a particle which had a speed in the x direction of v_{0x} in the first well will have a speed in the x direction of $v_x = \sqrt{v_{0x}^2 + \frac{2q}{m}(\phi_{ext} - \phi(x))}$ within the second well, neglecting the effect of collisions. Assuming q is positive, if $\phi_{ext} > \phi(x)$ no particles will exist at x with v_x between $-v_a$ and v_a, where $v_a = \sqrt{2q(\phi_{ext} - \phi(x))/m}$. Therefore, the distribution of particles at x will be

$$f(x,v) = n(\frac{\beta}{\pi})^{3/2} e^{-\beta(v^2 - \frac{2q}{m}(\phi_{ext}-\phi(x))}[\Theta(-v_x - v_a) + \Theta(v_a - v_x)]$$

if $\phi_{ext} > \phi(x)$ and

$$f(x,v) = n(\frac{\beta}{\pi})^{3/2} e^{-\beta(v^2 - \frac{2q}{m}(\phi_{ext}-\phi(x))}$$

otherwise. Note that if $\phi(x) = \phi_{ext}$ a Maxwellian distribution function if recovered. From this distribution function the density distribution within the second well may

be determined by integration over v. The result is

$$n(x) = ne^{q(\phi_{ext}-\phi(x))/T}\,\mathrm{erfc}(\sqrt{q(\phi_{ext}-\phi(x))/T}) \tag{2.4}$$

for $\phi_{ext} > \phi(x)$ and

$$n(x) = ne^{q(\phi_{ext}-\phi(x))/T} \tag{2.5}$$

otherwise.

Equations (2.4) and (2.5) may together be written as

$$n(x) = ne^{q(\phi_{ext}-\phi(x))/T}\,\mathrm{erfc}(\mathrm{Re}(\sqrt{q(\phi_{ext}-\phi(x))/T})).$$

This is the "antishielding" density distribution. This density distribution is shown for a $T = 1\,\mathrm{eV}$ plasma in a parabolic test well for various values of ϕ_{ext} in Fig 2.3. Note that the density reaches a maximum value at the location where $\phi = \phi_{ext}$, and the density at $\phi = 0$ is decreased with increasing ϕ_{ext}.

For the purposes of the self-consistent calculation, it is convenient to write the "antishielding" distribution in terms of the potential at the origin ϕ_0 and density at the origin n_0. The result is

$$n(x) = n_0 e^{q(\phi_0-\phi(x))/T}\frac{\mathrm{erfc}(\mathrm{Re}(\sqrt{q(\phi_{ext}-\phi(x))/T}))}{\mathrm{erfc}(\mathrm{Re}(\sqrt{q(\phi_{ext}-\phi_0)/T}))},$$

or if ϕ_{ext} is set equal to ϕ_0,

$$n(x) = n_0 e^{q(\phi_0-\phi(x))/T}\,\mathrm{erfc}(\mathrm{Re}(\sqrt{q(\phi_0-\phi(x))/T})).$$

Procedures for Establishing and Maintaining an Antishielding Distribution

Figure 2.4a shows an initial trap potential profile used to set up a nested well with one component in an antishielding distribution. Additional electrodes besides the five required to produce the nested well are needed to set-up or re-establish an

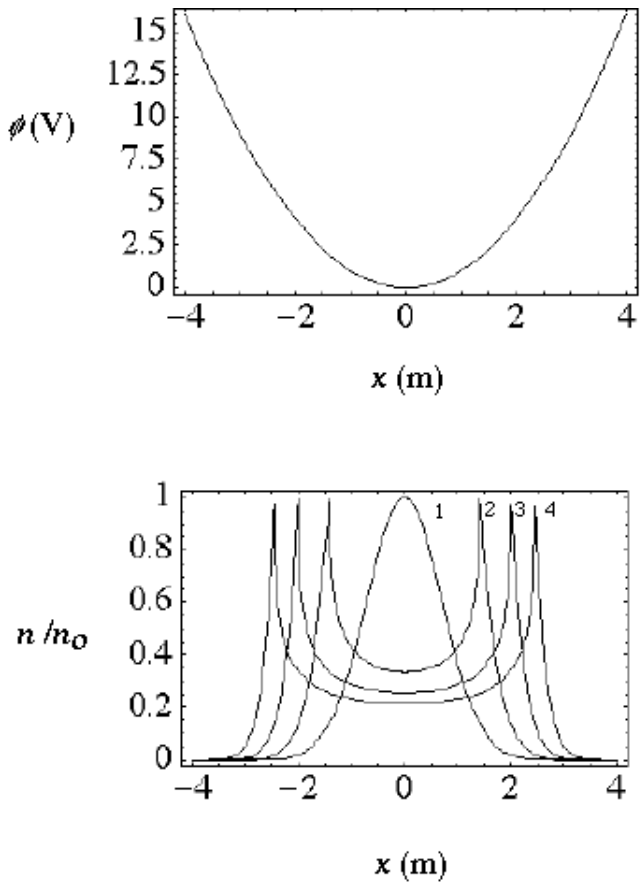

FIG. 2.3. An example of the density distributions associated with a $T = 1\,\mathrm{eV}$ positive plasma in an antishielding state. The top panel shows the potential well used for this example. The bottom panel shows the density distributions resulting from a plasma in an antishielding distribution with $\phi_{ext} = 0,2,4,6$ V in curves 1,2,3,4 respectively.

antishielding distribution. In this example a positively charged plasma species is confined within the inner well with an equilibrium distribution, and a negatively charged plasma component is confined outside of the nested well. Both species are at the same temperature. The barrier separating the negative species from the nested well can be dropped, allowing that species to flow into the nested well without compromising the confinement of the positive species, as indicated in Fig. 2.4b.

The plasma will only be in the antishielding state, as shown in Fig. 2.4c, immediately after entering the nested well. Collisions and possibly microinstabilities will begin to cause the plasma to relax to an equilibrium distribution and separate from the inner well plasma component.

To counteract this relaxation to equilibrium and maintain an antishielding distribution it will be necessary to have some time dependent manipulation of the potential. This can be accomplished by altering the potential in the manner demonstrated in Fig. 2.5. After the negative species has relaxed toward equilibrium and the two plasma components have begun to separate, as shown in Fig. 2.5a, the end wells and external electrodes can be set at some voltage that will allow the negative plasma to flow out of the nested well, as in Fig. 2.5b. It can then be trapped in a pair of potential wells external to the nested well, returned to the required starting potential, and cooled back to the starting temperature, Fig. 2.5c. The antishielding state may then be re-established by allowing the positive plasma to flow back into the nested well.

Plasma Confinement Properties

It will often be important to determine a timescale for a plasma's confinement within the nested well. The timescales determined may be compared to other

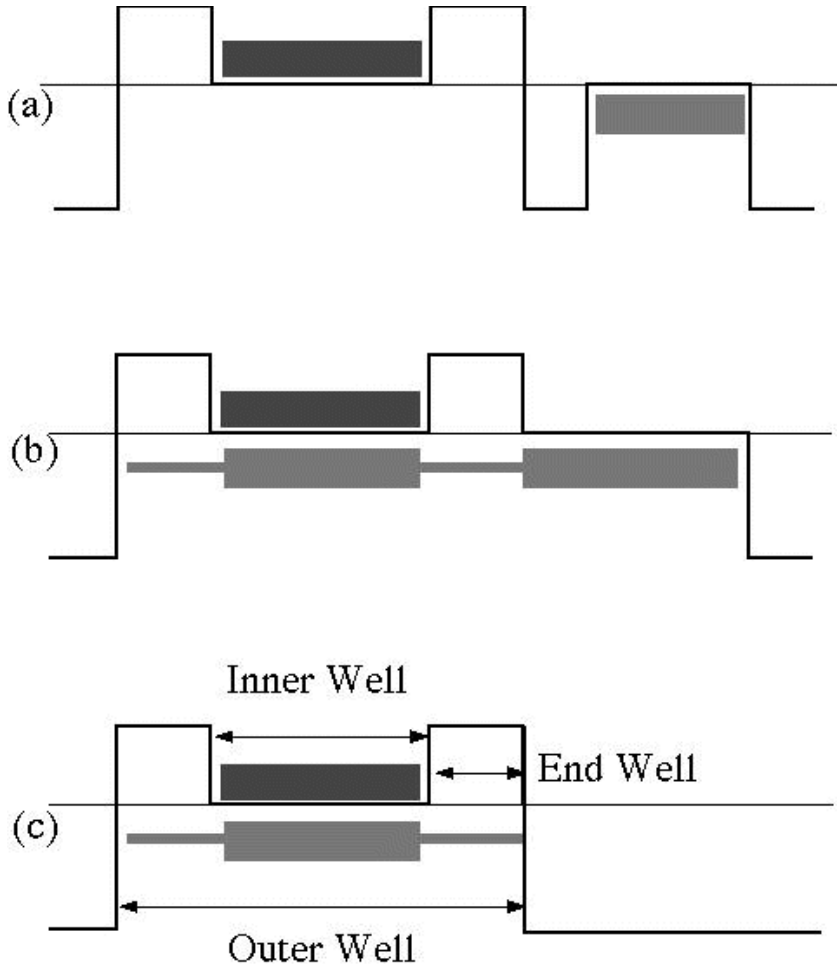

FIG. 2.4. The procedure for establishing a negatively charged plasma component in an antishielding state. (a) Initially the plasma components are separated and have thermal velocity distributions. (b) The barrier which prevents the negatively charged plasma from entering the nested well is removed and the negative plasma flows into the nested well. (c) The potential profile is reverted to the typical nested well profile leaving the negative plasma in an antishielding state which significantly overlaps the positive plasma. Eventually this plasma would relax to an equilibrium distribution and become trapped in the end wells.

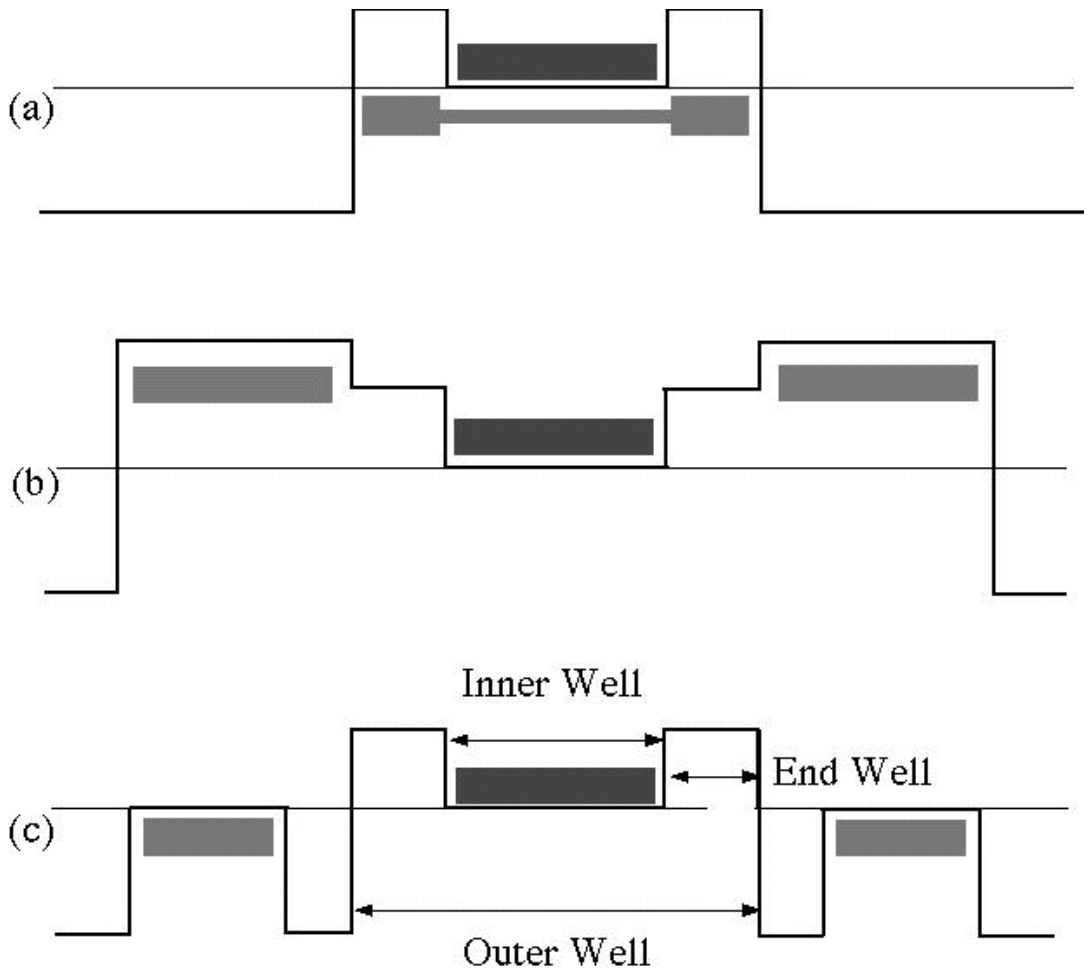

FIG. 2.5. A possible procedure for re-establishing an antishielding distribution. (a) The negative component has begun to relax and become trapped in the end wells. (b) Electrodes external to the nested well on either side are set at some voltage higher than the end well voltage. The negative plasma is allowed to equilibrate with this new well and become trapped in it. (c) The electrode voltages are altered so that the negative plasma is confined in a well at the same potential as the inner well. The plasma may then be cooled by various means so that the situation shown in Fig. 2.4(a) is recovered.

timescales relevant to the specific application to determine if the confinement voltages and axial magnetic field of the trap are adequate. Two different methods are used to evaluate axial and radial confinement properties.

Axial Confinement

The method used to determine an axial confinement timescale involves assuming a source of Maxwellian-distributed particles at a specified location in the trap. A phase space distribution consistent with this source is determined, and a particle flux escaping the trap can be calculated.[13–20] In this section it is assumed that the nested well trap is established such that the positive plasma species is confined in the inner well, and the negative species is confined by the outer well. However, this choice is only made for convenience, and the results apply equally to an inverted well with the plasma signs exchanged. The analysis in this section is carried out in one dimension (along a magnetic field line) so no r dependence is explicitly considered.

For the negative species a particle source is assumed to be at the location of the maximum trap potential ($z = z_m$) along the magnetic field line considered. Maxwellian-distributed particles are emitted from this source in the positive z direction. Between z_m and z_w, the location of the end of the trap, the phase-space distribution of these particles is,

$$f_-(z, \mathbf{v}) = n_{0-} \left(\frac{\beta_-}{\pi}\right)^{3/2} \exp\left(-\beta_- v^2 - \psi_-(z) + \psi_-(0)\right) \Theta(v_m + v_z),$$

where $v_m = \left[\left(\psi_-(z) - \psi_-(z_w)\right)/\beta_-\right]^{1/2}$ is the minimum speed in the positive z direction that allows a particle to reach z_w, $\beta_- = m_-/(2T_-)$, m_- is the mass of a particle of the negative plasma, T_- is its temperature in energy units, and $\psi_-(z) = q_-\phi(z)/T_-$. The Heaviside step function is included because any particle

with a velocity in the z direction greater than v_m will escape axially. For simplicity it is assumed that the negatively charged particles are Maxwellian in the region $0 < z < z_m$. In the limit that $\phi(z_w) \to -\infty$, $v_m \to \infty$ and perfect axial confinement is achieved. In this limit the phase space distribution becomes a Maxwell-Boltzmann distribution.

A density distribution can be obtained by integrating f_- over velocity space. For $z_m < z < z_w$ the result is

$$n_- = \frac{1}{2} n_{0-} \exp(-\psi_-(z) + \psi_-(0)) \mathrm{erfc}\left(-\sqrt{\psi_-(z) - \psi_-(z_w)}\right).$$

Integrating $v_z f_e$ over velocity space and evaluating at $z = z_w$ gives the net flux of particles escaping confinement in the axial direction,

$$F_- = \frac{n_{0-} \exp(-\psi_-(z) + \psi_-(0))}{2\sqrt{\pi \beta_-}}.$$

Using the expressions for n_- and F_- an axial confinement time scale can be defined as

$$\begin{aligned}
\tau_- &= \frac{1}{F_-} \int_0^{z_w} n_-(z) dz \\
&= \frac{1}{F_-} \left[\int_0^{z_m} n_{0-} e^{-\psi_-(z) + \psi_-(0)} dz \right. \\
&\qquad \left. + \int_{z_m}^{z_w} \frac{1}{2} n_{0-} e^{-\psi_-(z) + \psi_-(0)} \mathrm{erfc}\left(-\sqrt{-\psi_-(z) + \psi_-(z_w)}\right) dz \right] \\
&= \sqrt{\pi \beta_-} e^{\psi_-(z_w)} \left[2 \int_0^{z_m} e^{-\psi_-(z)} dz + \int_{z_m}^{z_w} e^{-\psi_-(z)} \mathrm{erfc}\left(-\sqrt{-\psi_-(z) + \psi_-(z_w)}\right) dz \right].
\end{aligned}$$

This confinement time can be considered a lower bound. In reality a plasma will lose particles from the tails of the velocity distribution as this method considers. However, the tails will not be instantaneously replenished, as in this model, but will be replenished at a finite rate by collisions or microinstabilities.

To determine the axial confinement properties of the inner well plasma species an analogous method is used. For the inner well species a source located at $z = 0$ is considered. Inner well particles are lost from the distribution if they reach $z = z_m$. The phase-space distribution of inner well particles is

$$f_+ = n_{0+} \left(\frac{\beta_+}{\pi} \right)^{3/2} e^{-\beta_+ v^2 - \psi_+(z) + \psi_+(0)} \Theta \left(v_m + v_z \right).$$

In this case $v_m = \left[\left(\psi_+(z_m) - \psi_+(z) \right) / \beta_z \right]^{1/2}$ is the minimum velocity required to reach z_m and $\psi_+(z) = q_+ \phi(z)/T_+$. The density of the positive species is obtained by integration as before, giving the result

$$n_+(z) = \frac{1}{2} n_{0+} e^{-\psi_+(z) + \psi_+(0)} \mathrm{erfc} \left[-\sqrt{\psi_+(z_m) - \psi_+(z)} \right].$$

The flux obtained is

$$F_+ = \frac{n_{0+} e^{-\psi_+(z_m) + \psi_+(0)}}{w \sqrt{\pi \beta_+}}.$$

From these quantities the confinement time is

$$\begin{aligned} \tau_+ &= \frac{1}{F_+} \int_0^{z_m} n_z(z) dz \\ &= \sqrt{\pi \beta_+} e^{\psi_+(z_m)} \int_0^{z_m} e^{-\psi_+(z)} \mathrm{erfc} \left[-\sqrt{\psi(z_m) - \psi(z)} \right] dz. \end{aligned}$$

It should be noted that for a series of cylindrical electrodes with no plasma present, any electric potential step created will be largest at the electrode surface. Due to geometrical effects the potential step along the $r = 0$ line will be smallest. If an equilibrium plasma is introduced, it will shield the center of the cylinder, further decreasing any potential step. For these reasons, the potential step along the $r = 0$ line may be considered as providing the least effective axial confinement. If a plasma has adequate axial confinement along the $r = 0$ line, good axial confinement along all magnetic field lines may be assumed.

Radial Confinement

An additional concern is the loss of particles in the radial direction. Throughout the volume of the trap a constant magnetic field exists. This field serves to keep both positive and negative plasma particles from intersecting the electrode walls. In the absence of any electrical fields the motion of both positive and negative particles would be a helix about a magnetic field line with radius equal to the Larmor radius, $r_L = mv_\perp/(|q|B)$. In a trap with a radial component to the electric field, the trajectory of a particle becomes a superposition of $\mathbf{E} \times \mathbf{B}$ drift and helical motion. Given an electrical field proportional to r, an exact solution can be obtained. See Chap. 1. However, within a nested well trap the self-consistent potential will not be this simple, and numerical methods must be used to evaluate confinement properties. This method makes no attempt to model interactions between particles. Instead, classical single particle trajectories are calculated for particles in the self consistently determined electric field, resulting from both electrode and plasma contributions.

Radial confinement is a much more important issue for heavier plasma components because they have a larger Larmor radius. Generally, the numerical method described in this section will be applied to heavy ionic plasma components, although it could be used for lighter plasma components. This method involves Monte Carlo sampling of Maxwellian velocities using the following equations for particle i :

$$v_{zi} = \frac{\mathrm{erf}^{-1}(R_{1i})}{\sqrt{\beta_i}}$$

and

$$v_{\perp i} = \sqrt{\frac{-\ln(R_{2i})}{\beta_i}},$$

where R_{ni} is a uniformly distributed random number between 0 and 1. The equation for v_z samples from a half-Maxwellian distribution so that v_z will always be given

a positive value initially. The particular azimuthal direction for $v_\perp$ is chosen with a uniform distribution of angles from 0 to 2π. The particle is initially located in the $z = 0$ plane. An initial radial position is sampled from $r_i = r_w\sqrt{R_{3i}}$, which provides for an evenly distributed starting point within a circle of radius $r_{w.}$ The code then calculates the Larmor radius, r_L, for the particle and the location of the guiding center of the particle r_c. If the sampled values are such that $r_L + r_c \geq r_w$, the particle will intersect the electrode wall without the effect of any radial electric field. To reduce computational time, these particles are discarded before any further computation occurs.

For each set of initial conditions which are not discarded, a trajectory is solved for numerically, assuming a uniform magnetic field and an electric potential which was previously calculated with an SOR code. This trajectory is followed until the particle either returns to the $z = 0$ plane after one or more passes through the trap or escapes confinement radially or axially. Additionally, a few particles may be selected with very low v_z and take a long time to traverse the trap. To keep the computation time manageable, no particle is followed for more than a specified maximum number of computation time steps. The code maintains lists of which initial conditions result in confinement and which result in escape. This code is given in Appendix C. By carrying out calculations for a large number of particles, radial confinement statistics may be generated, and regions of phase space from which losses occur can be identified. These may be compared with the phase space distribution assumed for the purposes of the self-consistent calculation.

REFERENCES

[1]D. H. Dubin and T. M. O'Neil, "Trapped nonneutral plasmas, liquids, and crystals (the thermal equilibrium states)," Reviews of Modern Physics **71**, 87 (1999).

[2]D. S. Hall and G. Gabrielse, "Electron cooling of protons in a nested Penning trap," Phys. Rev. Lett. **77**, 1962 (1996).

[3]G. Gabrielse, S. l. Rolston, L. Haarsma, and W. Kells, "Antihydrogen production using trapped plasmas," Phys. Lett. A **129**, 38 (1988).

[4]C. A. Ordonez, "Confinement of a neutral plasma using nested electric potential wells," Phys. Plasmas **4**, 2313 (1997).

[5]C. Hansen, A. B. Reimann, and J. Fajans, "Dynamic and Debye shielding and anti-shielding.," Phys. Plasmas **3**, 1820 (1996).

[6]C. Hansen and J. Fajans, "Dynamic and Debye shielding and antishielding in magnetized, collisionless plasmas," Phys. Rev. Lett. **74**, 4209 (1995).

[7]C. A. Ordonez, "Time-dependent nested-well plasma trap," IEEE Trans. on Plasma Sci. **24**, 1378 (1996).

[8]R. L. Spencer, S. N. Rasband, and R. R. Vanfleet, "Numerical calculation of axisymmetric non-neutral plasma equilibria," Phys. Fluids B **5**, 4267 (1993).

[9]S. A. Prasad and T. M. O'Neil, "Finite length thermal equilibria of a pure electron plasma column," Phys. Fluids **22**, 278 (1979).

[10]A. J. Peurrung and J. Fajans, "Non-neutal plasma shapes and edge profiles," Phys. Fluids B **2**, 693 (1990).

[11]R. L. Spencer and G. W. Hart, "Linear theory of non-neutral plasma equilibrium in a tilted magnetic field," Phys. Fluids B **4**, 3507 (1992).

[12]W. H. Press, *Numerical Recipes in FORTRAN*, Cambride University Press, New York., 1992.

[13]L. A. Schwager and C. K. Birdsall, "Collector and source sheaths of a finite ion temperature plasma," Phys Fluids B **2**, 1057 (1990).

[14]L. A. Schwager, "Effects of secondary and thermionic electron emission on the collector and source sheaths of a finite ion temperature plasma using kinetic theory and numerical simulation," Phys. Fluids B **5**, 631 (1993).

[15]C. A. Ordonez, "Fully kinetic plasmas-sheath theory for a cold-electron emitting surface," Phys. Fluids B **4**, 778 (1992).

[16]C. A. Ordonez, "Effect of a plasma sheath and ion injection on axial particle and energy confinement in a collisional mirror plasma," Phys. Plasmas **1**, 1359 (1994).

[17]K. Kurihara, Y. Kiwamoto, T. Saito, K. Yatsu, and S. Miyoshi, "Study of potential formation in an open magnetic field configuration," J. Phys. Soc. Jpn. **61**, 3153 (1992).

[18]T. Saito et al., "Scaling study of potential in the end region of a tandem mirror based on end-loss electron measurement," Phys. Fluids B **5**, 866 (1993).

[19]Y. Tatematsu, Y. Kiwamoto, T. Saito, and T. Tamano, "Effects of Yushmanov-trapped particles and anisotropy of velocity distribution on the potential formation in the end region of the tandem mirror," J. Phys. Soc. Jpn. **63**, 558 (1994).

[20]Y. Tatematsu et al., "Control of plasma transport by active tailoring of potential profile along open magnetic fields," J. Nucl. Mater **220-222**, 575 (1995).

CHAPTER 3

USE OF A NESTED WELL TRAP AS A SOURCE OF HIGH-Z IONS

A possible application of a nested well plasma trap is as a source of high charge state ions. This device would in many ways be similar to existing electron beam ion sources (EBIS).[1] An EBIS uses a high energy electron beam which makes a single pass through a region containing ions. The ions are axially confined in an electric potential well and radially confined by the space charge of the electron beam. The electron beam is responsible for stripping the ions, and extremely high charge states can be produced.[2]

The charge states capable of being created by the nested well approach are limited by the temperature of the electrons which can be confined. However, the high charge state plasma produced by a nested well trap may have a thermal velocity distribution, and the plasma within the inner well of the trap may be neutral. Along with potentially serving as an ion source, a well confined, thermal, neutral, high charge state plasma would allow for the study of plasma recombination and transport processes.

The ions will be confined axially within the inner well by positively biasing the inner electrodes with respect to the central electrode. The electrons will be axially confined within the end wells by the negatively biased outer electrodes. If the electrode voltages are correctly selected, the electrons will significantly overlap the inner well. To allow for this overlap, the magnitude of the potential step between the center and inner electrode must be significantly smaller than the magnitude of

the potential step between the inner and outer electrode. Confinement of the ions within the inner well will still be possible in this case.

Initially, the trap will be loaded with very high temperature electrons and cold low charge state ions, and the ions will not have enough thermal energy to escape the inner well. As the electrons exchange energy with the ions and the ion temperature increases, the ions will also become more highly ionized. Therefore, the ions will feel a larger potential step between the region of the center and inner electrodes and will remain adequately confined even though their temperature has increased.

Details of the Self-Consistent Calculation

A series of calculations of a nested well trap operating with a high charge state argon plasma has been carried out. The base parameters used for most calculations are described below and listed in Table 3.1. Some computational experiments have also been performed in which one or more of the values of the parameters have been changed from those given in the table. Estimates of the charge spectrum of argon at various temperatures have been obtained using the corona model.[3] The corona model assumes that the opposing processes of collisional ionization and radiative recombination are dominant. The equilibrium charge state ratios predicted by this model are given by

$$\frac{N_Z}{N_{Z+1}} = 7.87 \times 10^{-9} \left(\frac{U_Z}{e}\right)^2 \left(\frac{U_Z}{T}\right)^{3/4} e^{U_Z/T}.$$

Fig. 3.1 shows the average charge state predicted versus temperature for both argon and neon. Notice that it is energetically easier to achieve a given charge state with argon as opposed to neon. In general, the greater the atomic number the easier it is to achieve a given charge state because the outer electrons of the higher atomic

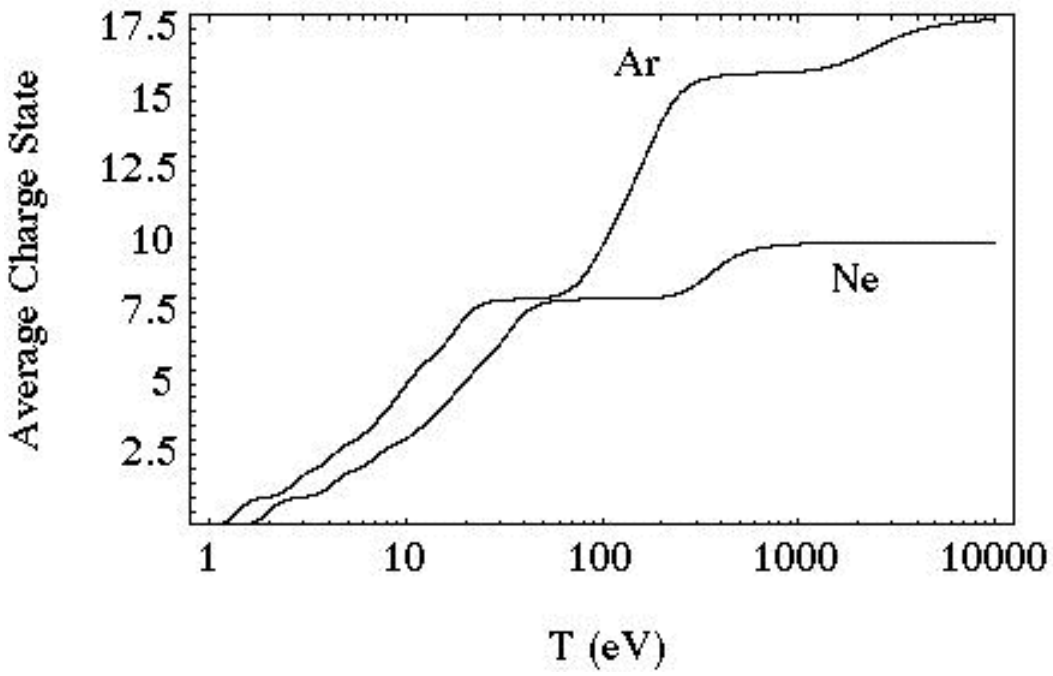

FIG. 3.1. The average charge state predicted by the corona model for both argon and neon plasmas versus temperature.

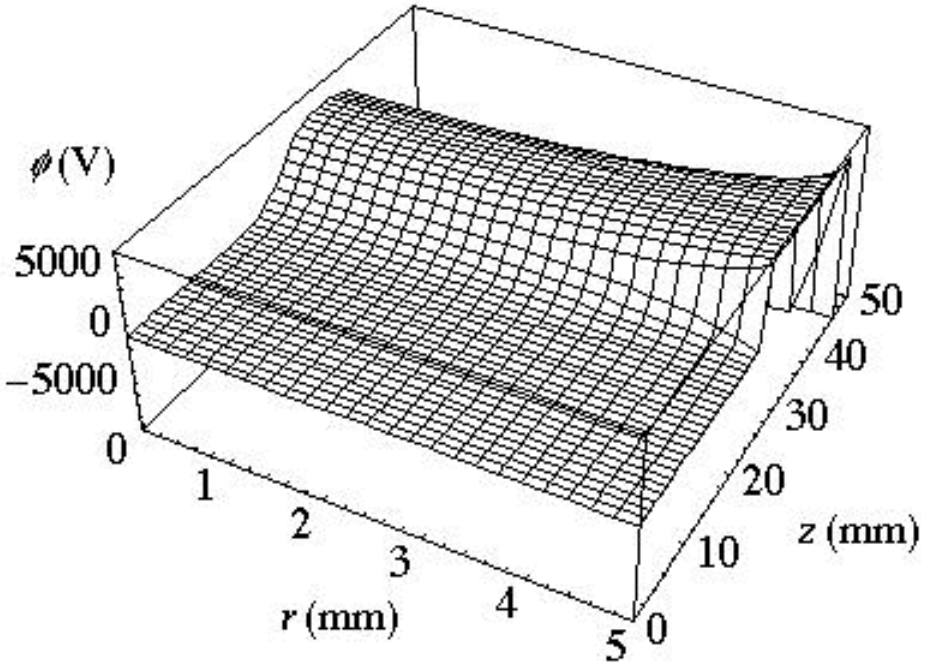

FIG. 3.2. The self-consistently calculated potential for a nested well trap using the parameters given in Table 3.1.

number species are typically less strongly bound. According to the corona model, to obtain an argon plasma with the largest percentage of the ions fully-stripped (charge state +18), it is necessary to use a temperature of approximately 3 keV. At this temperature the corona model charge spectrum of argon is 39.9% charge state +18, 36.0% charge state +17, and 24.1% charge state +16. All other charge states amount to less than 0.1% of the total and will be neglected in the computation. The average charge state is +17.2.

With plasmas at a temperature of 3 keV, the voltages V_1 and V_2 are set at 6.7 kV and -82 kV respectively to provide adequate confinement. The axial magnetic field B is set to 10 T. The electrode lengths are set at $L_0 = 5$ cm, $L_1 = 2$ cm, and

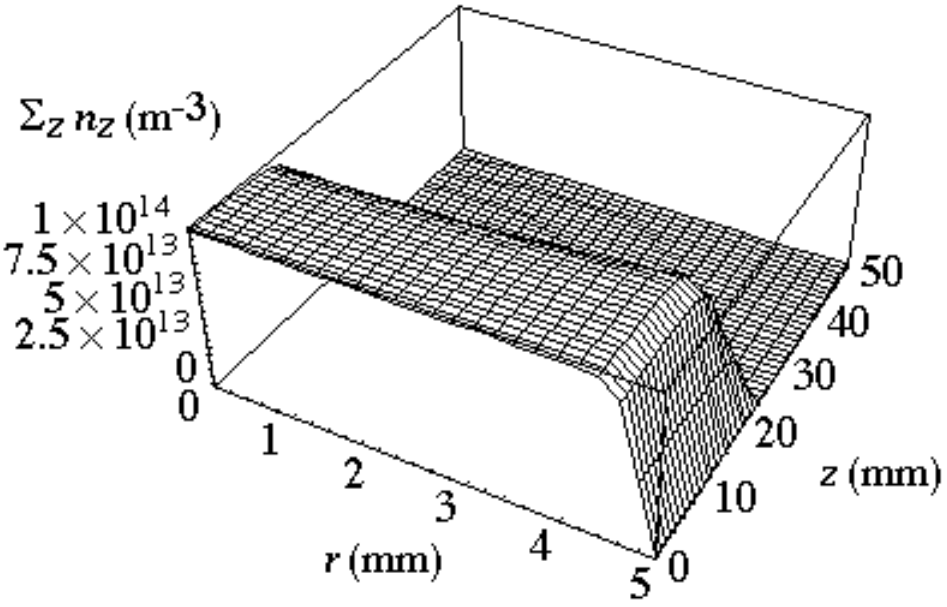

FIG. 3.3. The self-consistently calculated ion density distribution showing that the ions are trapped within the inner well.

$L_2 = 0.5$ cm. The electrode separation is neglected (set at a distance smaller than the grid spacing). The radius of the trap is set at $r_w = 0.5$ cm. The central density of the ion plasma component, $\sum_z n_z(0,0)$, is set at 10^{14} m^{-3}; the central electron density is set at $1.72\times\ 10^{15}$, which will result in neutrality along $z = 0$. It should be noted that by using such high voltages and small gaps between electrodes, large electric fields are produced. In an actual experiment it will be necessary to increase the electrode separation to prevent surface breakdown.

The ions are assigned the density distribution given by Eq.(2.3) within the inner well. Outside of the inner well they are unconfined, and their density is set to zero. It has been noted that including this type of artificial cutoff in a plasma

component's density is always necessary to prevent the occurrence of the plasma beyond the confining electrode.[4] As the axial position approaches the potential step created by the inner well electrode, the ion density becomes very small without the cutoff. In fact, because Eq. (2.3) is used, the ion density will be zero at the top of the potential step where $\phi(r,z) = \phi_m(r)$. However, without the cutoff, the ion density in the region beyond the inner well electrode, $|z| > 4.5\,\mathrm{cm}$, would be non-zero. Several methods for implementing this cutoff are possible. Among these are finding the grid point along each radial line at which the maximal potential occurs and setting the ion density equal to zero for axial positions beyond that or simply setting a fixed cutoff position, e.g., the start of the inner well electrode, $z = 2.5\,\mathrm{cm}$. As the ion density is very nearly equal to zero before reaching the region of the inner well electrode, the exact method of cutoff chosen makes little difference in the solution. Therefore, for simplicity a fixed cutoff at $|z| = 2.5\,\mathrm{cm}$ is chosen. Equation (2.3) excludes from the distribution those particles which have gyro-orbits which will intersect the electrode walls as well as those particles which will not be axially confined.

The electron density profile is given by $n_e(r,z) = n_e(r,0)\exp(e(\phi(r,z)-\phi(r,0))/T)$. The electrons follow the Boltzmann relation in the axial direction for each radius. The boundary condition $n_e(r,0)$ must be specified. If any charge separation occurs within the inner well, the radial field produced can be expected to cause a radial diffusion of the electrons. In a trap with $L_0 \gg L_1$ the effect is that the plasma will be highly neutral along the $z = 0$ plane. Because of this, $n_e(r,0)$ is set equal to the radial profile of the ion plasma so that a neutral plasma results along the $z = 0$ plane. In the example calculation $L_0/L_1 = 2.5$; however, the results generated are

Table 3.1. Parameter values used for the calculation of the electric potential and plasma density distributions in a nested well plasma trap confining electrons and high charge state argon.

Parameter	**Value**
r_w	0.5 cm
L_0	5 cm
L_1	2 cm
L_2	0.5 cm
V_1	6.7 kV
V_2	-82 kV
$\Sigma_Z n_Z(0,0)$	10^{14} m^{-3}
$n_e(0,0)$	1.72×10^{15} m^{-3}
B	10 T
T	3000 eV
Average Ion Charge State	+17.2

expected to be even more representative of a trap with $L_0/L_1 > 2.5$.

The self-consistently calculated results for the parameters shown in Table 3.1 are shown in Figs. 3.2-3.5. Figure 3.2 shows the electric potential within the trap. Along the electrode wall the potential is equal to the applied electrode potential. At smaller radii the potential is much smoother and the magnitude of the potential wells are lessened, which occurs both from geometrical effects and plasma shielding

Figure 3.3 shows the self-consistently determined ion density distribution. The 10 T magnetic field which was used allows the ion density to be radially flat out to very near the radial electrode wall. Although a step function was included to set the ion density to zero outside of the inner well, at $z > 2.5$ cm, the ion density falls to near zero well before that. The step function has no effect other than to prevent the appearance of an ion plasma in the region near the end electrode ($z > 4.5$ cm).

Figure 3.4 shows the electron density distribution. The electrons have a much greater density within the end wells; however, their density is non-zero within the

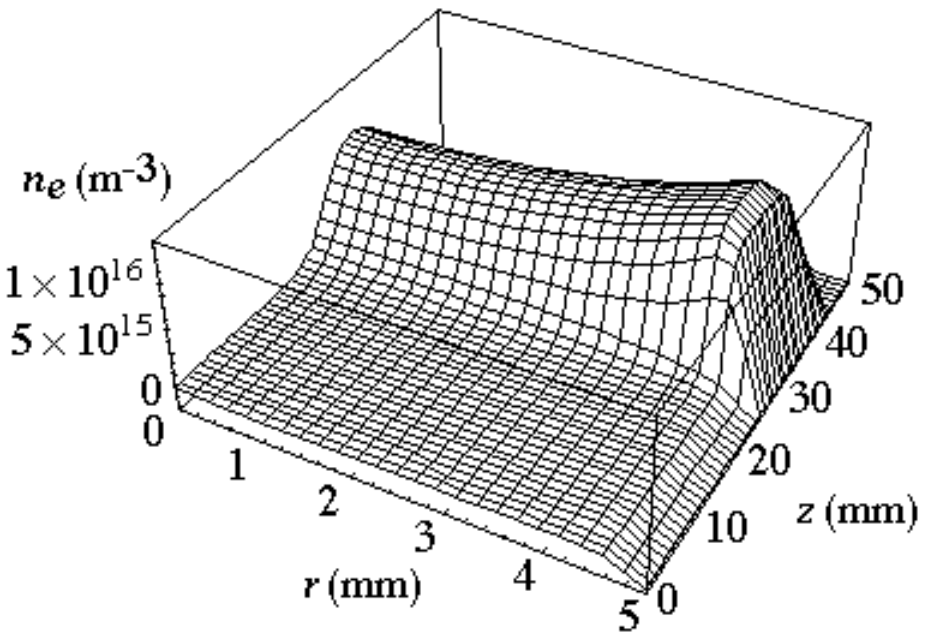

FIG. 3.4. The self-consistently determined electron density. The electrons are largely trapped in the end well, but they significantly overlap the inner well.

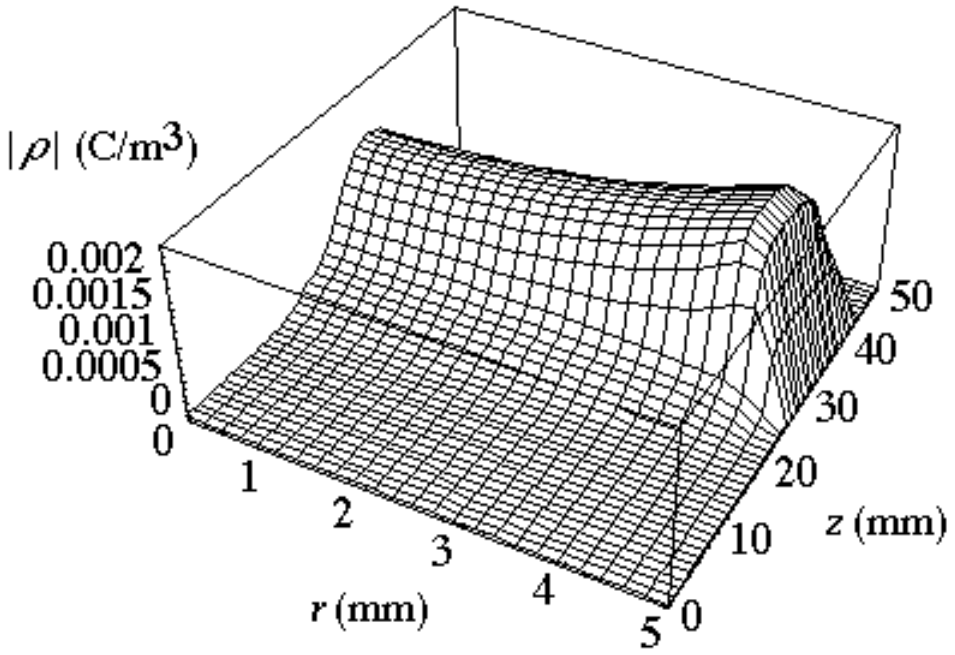

FIG. 3.5. The magnitude of the charge density demonstrating that the inner well region is neutral.

inner well. In fact, they overlap the ions significantly enough to neutralize the ion space charge within the inner well almost completely. This is shown in Fig. 3.5, a plot of the magnitude of the charge density throughout the trap.

Because the end well region is nonneutral, Debye shielding is responsible for reducing the depth of the end well. The larger the electron density, the more the end well depth is reduced. This is demonstrated in Fig. 3.6.

Axial Confinement of Ions and Electrons

Using the planar source method for calculating ion and electron confinement times that was discussed in the previous chapter, minimum confinement times for ions and electrons may be calculated. These times are estimated using the self-

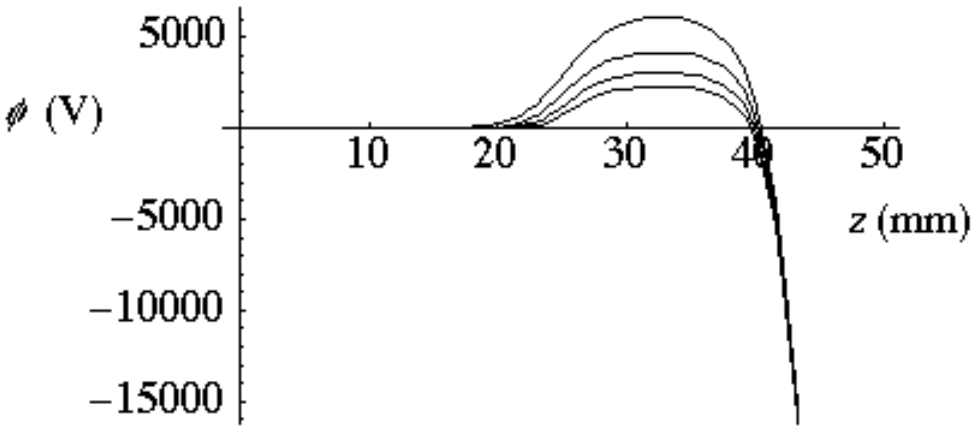

FIG. 3.6. The electric potential on the trap axis for a trap with no plasma (the top curve) and plasma densities of $n_{0e} = \sum_z n_{0z} = 2.5 \times 10^{14}$, 5.0×10^{14} , 7.5×10^{14} m^{-3}. This demonstrates the Debye shielding of the end well.

consistently calculated potential along the $r = 0$ magnetic field line which is least confining. For the parameters listed in Table 3.1 a confinement time for both electrons and +18 charge state ions is estimated to be approximately 2 hours. This value is large enough that each plasma component may be considered perfectly confined axially.

Radial Ion Confinement

The confinement of both ions and electrons in the radial direction is achieved via the 10 T magnetic field. At a temperature of 3 keV, the Larmor radius of an electron in a 10 T field is 1.85×10^{-5} m, and the Larmor radius of an argon ion with charge state +17 is 2.95×10^{-4} m. By comparing with the trap radius of .05 m, it is easy to see that the effect of the intersection of Larmor orbits with the wall is only important for particles very near the wall. A further concern is the effect the radial electric field present in the trap will have on radial confinement. The radial component to

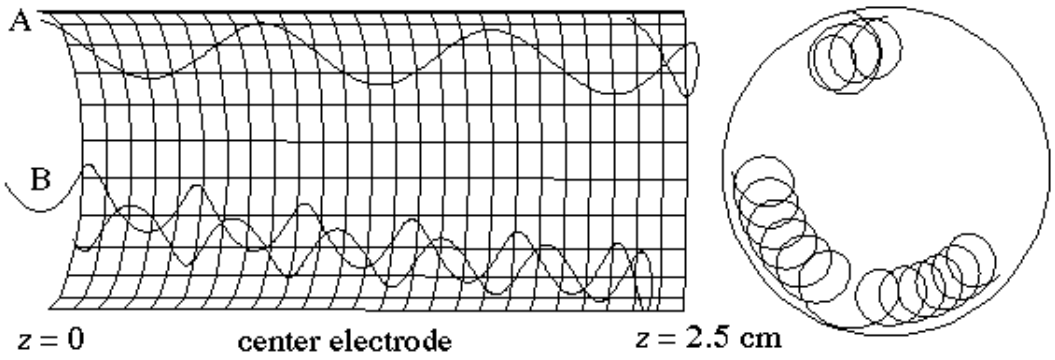

FIG. 3.7. Two single particle trajectories for +17 charge state ions calculated by the ion orbit code. The initial conditions are identical except that the escaping particle has twice the axial velocity of the confined particle and consequently it spends more time in the high radial field region of the trap.

the electric field is particularly important near the boundaries between electrodes, but it should be reiterated that because the gaps between electrodes were neglected in the SOR calculation the magnitude of the electric fields is exaggerated.

A calculation of the orbits of ions with the ion orbit code described in Appendix C has been implemented. Single particle trajectories for ions starting at the midplane of the trap with velocities sampled from a half-Maxwellian velocity distribution are calculated. Note that particles whose initial velocities would result in gyro-orbits that would intersect the electrode walls are excluded by the code before the orbit is calculated. This results in a distribution of particles that is approximately the same as that used for the self-consistent calculation of the potential, only differing in that the distribution used for the self-consistent calculation, Eq.(2.2), used the guiding center approximation. That is, in calculating the potential the approximation that $r = r_c$ was made. Figure 3.7 shows sample orbits calculated from two initial conditions that differ only by having a different axial velocity.

The single particle trajectories of 10,000 +17 charge state ions have been cal-

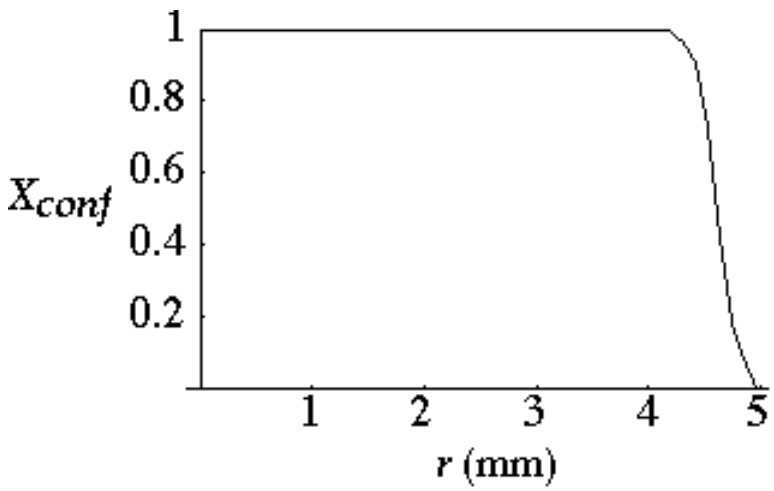

FIG. 3.8. The fraction of orbits which remain confined during one pass in the trap, X_{conf}, versus initial radial position of the particle.

culated. The fraction of particles which remain confined for one pass through the trap versus the initial radial position of the particle are shown in Fig. 3.8. Overall, the calculations show 94% of the initial conditions lead to confinement for one pass. Essentially, all trajectories that lead to loss come from initial conditions within one millimeter of the wall. If larger electrode gaps are used the magnitude of the electric field, particularly near the electrode wall and near the gaps, can be expected to be much smaller. This calculation is expected to overestimate the number of single particle trajectories that lead to loss, particularly near the walls.

Concluding Remarks

Between the inner and outer well regions of the trap there is a transition between a neutral plasma region and a nonneutral one. Because of this transition there will be a shear in the $\mathbf{E} \times \mathbf{B}$ flow. A collisional torque between the electron plasma in the end well and the neutral plasma in the inner well will occur. This torque can be expected to primarily effect the electrons and cause radial diffusion within the end

wells.

However, it should be possible to achieve near perfect axial confinement of both species. "Rotating" field techniques have been developed which may make near perfect radial confinement possible.[1] Such a field could be applied to one end well region and would tend to radially compress the electron plasma. Within the inner well this will set up a radial electric field that tends to provide enhanced radial confinement of the ions.

REFERENCES

[1]H. Haseroth and C. E. Hill, "Multicharged ion sources for pulsed accelerators (invited)," Rev. Sci. Instrum. **67**, 945 (1996).

[2]R. E. Marrs, S. R. Elliot, and D. A. Knapp, "Production and trapping of hydrogenlike and bare uranium ions in an electron beam ion trap," Phys. Rev. Lett. **72**, 4082 (1994).

[3]W. P. McWhirter, "Spectral intensities," , in *Plasma Diagnostic Techniques*, edited by R. H. Huddlestone and S. L. Leonard, New York, 1965, Academic Press.

[4]R. L. Spencer, S. N. Rasband, and R. R. Vanfleet, "Numerical calculation of axisymmetric non-neutral plasma equilibria," Phys. Fluids B **5**, 4267 (1993).

CHAPTER 4

THREE-DIMENSIONAL ELECTRIC CONFINEMENT OF HIGH-CHARGE STATE PLASMAS

In Chapter 3 an analysis was presented of the use of a Penning trap with nested electric potential wells as a source of high-Z ions. Radial confinement of both species was achieved with an axial magnetic field, and the overlap region considered was neutral. In this chapter, an extension to that work is presented in which a more dense overlapping electron plasma is considered. Consequently, the overlap region considered is filled with a negative space charge, and a three-dimensional electric potential well results. This well provides confinement for the ions in both the axial and radial directions. In the scenario considered in this chapter the magnetic field is only responsible for the radial confinement of the electrons.

It should be noted that radial confinement with a magnetic field is possible in a situation where the particle cyclotron radius is smaller than the plasma radius. The less massive electrons have a smaller cyclotron radius and consequently may be confinable with a much smaller magnetic field. In Chap. 3 a 10 T magnetic field was considered to provide confinement for both ions and electrons. In this chapter a magnetic field of only 0.2 T is considered.

Consider a nested well Penning trap with an electrode configuration as shown in Fig. 2.1 with voltages selected so as to confine ions within the inner well and to confine electrons primarily within the end wells but allow the electrons to overlap the inner well. As has been discussed in Chap. 2 there are two scenarios in which a

significant overlap of two thermal components occurs within the inner well. Either the inner well component must be more highly charged than the outer well component or the outer well component must be significantly hotter than the inner well plasma.

With the proper choice of parameters the overlap may be significant enough so that the inner well region is neutral or even has a negative space charge. If the inner well region carries enough of a negative charge, the ions can be confined axially by the externally applied potential and confined radially by a radial electric potential well created by the electrons.

In the scenario with two different temperature components, if the two components are allowed to thermalize, they will separate, and a time dependent procedure will be necessary to maintain overlap. With the case of disparate charge state a region of overlap may be maintained with static fields.

Self-Consistent Calculation of Three Dimensional Electric Confinement

An example of a plasma in a nested well Penning trap confined in three dimensions by an electric potential well is shown in Figs. 4.1 to 4.3. This solution was created by the simultaneous over-relaxation numerical method described in Chap. 2 that self-consistently solves for the trap potential and particle distributions. The particular solution shown is for a high charge state argon plasma overlapped by equal temperature electrons. The plasma temperature used is 3 keV. The corona model argon charge state distribution at this temperature is given in Chap. 3. For convenience the solution in the present chapter was generated with a single ion species having the average charge state of +17.2.

The ion density at the geometric center of the trap is chosen to be $1 \times 10^{14}\,\mathrm{m}^{-3}$.

The electron density is set at $2 \times 10^{16}\,\mathrm{m}^{-3}$ at the center of the trap. The radial profile of the electrons is assumed to be $h(r) = 1 - (r/r_w)^{\alpha}$ at the midplane, where $\alpha = -2.3\ln(1 - \lambda_D/r_w)$. This profile holds the electron density fairly constant until within a few Debye lengths of the wall where it falls rapidly to zero. The ions are assumed to be in global thermal equilibrium; that is, they follow the Boltzmann relation both axially and radially within the inner well. The electrodes all have a radius of 5 mm. The central electrode is 5 cm long and grounded. The electrodes on either side of the central electrode are each 2 cm long and are held at 6.7 kV. The outermost electrodes are each 1 cm long and held at -82 kV.

The potential which results from this choice of parameters is shown in Fig. 4.1. The space charge of the electrons provides an electric potential well capable of providing radial confinement. The self-consistently determined ion density is shown in Fig. 4.2. The electron density is shown in Fig. 4.3.

For the parameters chosen, the ion cyclotron radius is 1 cm within the 5 mm radius trap. Thus, radial magnetic confinement of the ions is not possible. The electrons, however, have a cyclotron radius of .653 mm and may be radially confined by the magnetic field.

Evaluation of Limiting Ion Density

Note that, due to the Brillouin limit, it would require a 1.2 T magnetic field to confine argon ions at a density of $1 \times 10^{14}\,\mathrm{m}^{-3}$ in a nonneutral plasma trap. Because the inner well of the nested well trap considered in this Chapter has a negative charge density, the Brillouin density limit does not apply to the ions. Within the end wells the electron plasma is completely unneutralized and, consequently, is Brillouin limited. This limit on the electron density sets a limit on the maximum ion density

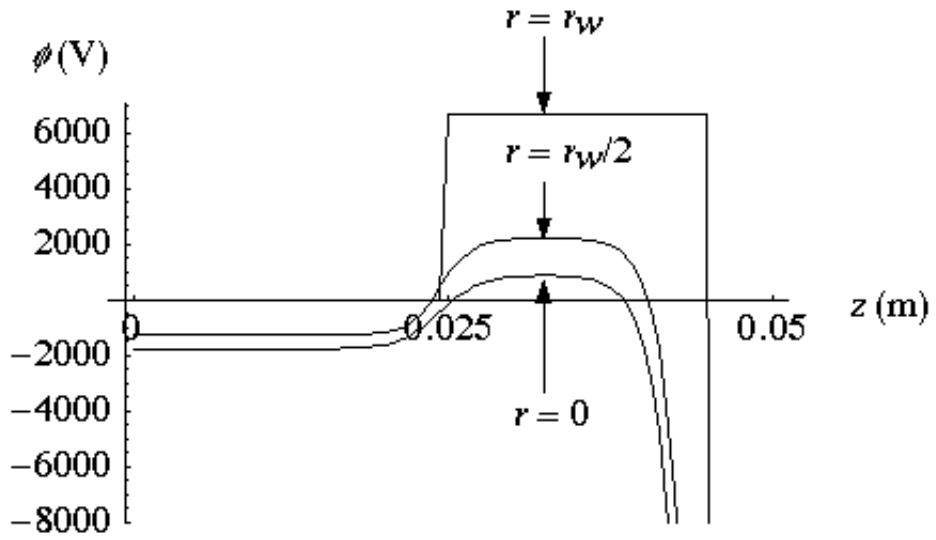

FIG. 4.1. The self-consistent potential with argon ions confined at a density above their Brillouin density limit in a nested well Penning trap.

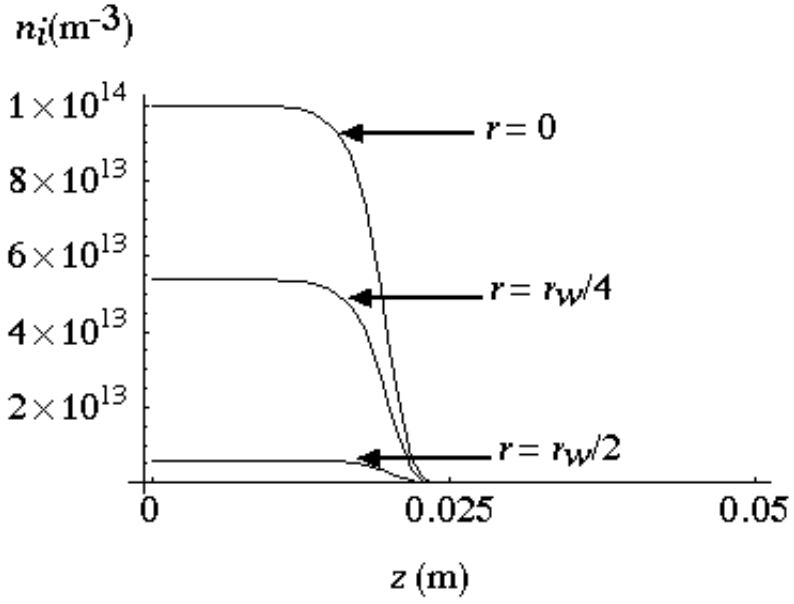

FIG. 4.2. The self-consistent density of argon ions in the trap.

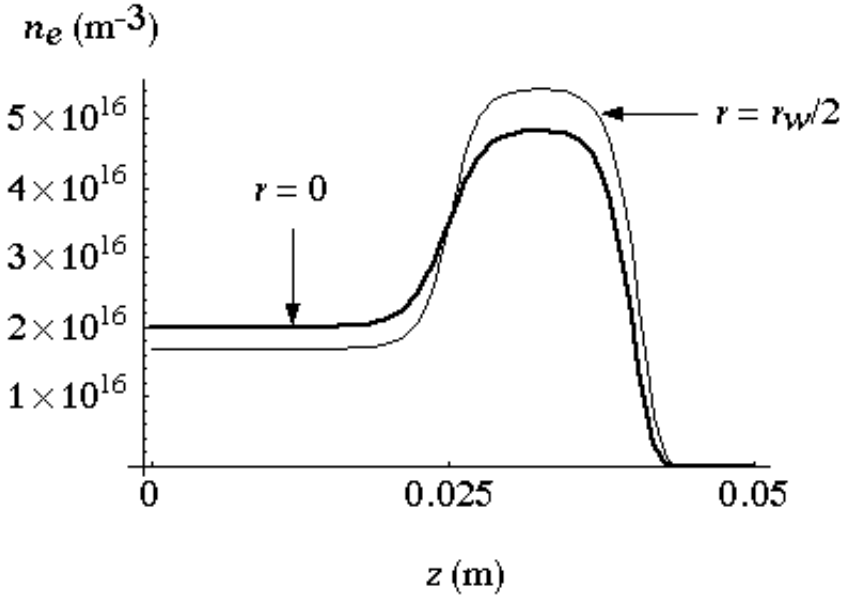

FIG. 4.3. The self-consistent density of electrons in the trap.

which may be confined within the inner well. An expression for the maximum ion density which may be confined, $n_{i,max}$, can be obtained. First, consider the electron density within the end well, $n_{e,ew}$, to be equal to the electron Brillouin limit, $n_{e,ew} = n_{Be} = \epsilon_0 B^2/(2m_e)$. As the electrons are considered to be in local thermal equilibrium the maximum electron density in the inner well is $n_{e,iw} = n_{e,ew} e^{-e\Delta\phi/T_e}$. We are considering a situation in which the inner well has a negative charge density so that the ions are confined by the resulting potential depression. However, we can consider as an upper limit the ion density which would result in neutrality within the inner well, $n_{i,max} = n_{e,iw}/Z$. In terms of the Brillouin ion density limit, n_{Bi}, the maximum ion density which may be confined is

$$n_{i,max} = \frac{m_i}{Z m_e} e^{-e\Delta\phi/T_e} n_{Bi}.$$

For the parameters considered in the self consistent computation, this evaluates to a maximum ion density of 1700 times the Brillouin limit. For the self-consistent calculation, the electron density in each end well is only approximately one fourth of the Brillouin electron density limit. The maximum ion density in the inner well is less than one tenth of the density that would result in a neutral plasma. As a result, the maximum ion density in the self-consistent calculation is only approximately 38 times the ion Brillouin limit.

REFERENCES

[1]H. Haseroth and C. E. Hill, "Multicharged ion sources for pulsed accelerators (invited)," Rev. Sci. Instrum. **67**, 945 (1996).

[2]R. E. Marrs, S. R. Elliot, and D. A. Knapp, "Production and trapping of hydrogenlike and bare uranium ions in an electron beam ion trap," Phys. Rev. Lett. **72**, 4082 (1994).

[3]W. P. McWhirter, "Spectral intensities," , in *Plasma Diagnostic Techniques*, edited by R. H. Huddlestone and S. L. Leonard, New York, 1965, Academic Press.

[4]R. L. Spencer, S. N. Rasband, and R. R. Vanfleet, "Numerical calculation of axisymmetric non-neutral plasma equilibria," Phys. Fluids B **5**, 4267 (1993).

CHAPTER 5

A PENNING TRAP WITH A RADIAL MAGNETIC FIELD

Typically a Penning trap consists of an electric potential well applied along a solenoidal magnetic field which is aligned with the trap axis. A trap in many ways similar to typical Penning traps can be created by aligning an electric potential well along a radial magnetic field. In fact, there is no reason why, in principle, a set of nested wells cannot be created along a radial magnetic field.

A region of radial magnetic field exists in a magnetic cusp configuration.[1] The Andreoletti-Furth configuration is a modification of the magnetic cusp in which a local magnetic minimum exists within the radial field region.[1,2] Such a trap is being considered for use in the problem of recombining and trapping antihydrogen atoms.[3] In Fig. 5.1 the trap system is shown. Azimuthal symmetry is assumed. There are six washer shaped electrodes separated by a distance $2z_w$. Between the two electrode surfaces a region of radial magnetic field exists. Consider an ion plasma of charge state Z to be confined between the electrodes. This plasma will be of width $2z_p$ and extend from $r = r_{pi}$ to $r = r_{po}$.

In this chapter this radial magnetic field configuration is considered as a method in which a nonneutral plasma in "local thermal equilibrium," that is a plasma which follows the Boltzmann relation along each magnetic field line, may be confined with a density in excess of the Brillouin limit. A plasma confined at a density exceeding the Brillouin limit may serve as the outer well plasma in a nested configuration. Previous experimental work has demonstrated ion confinement at the Brillouin limit.[4]

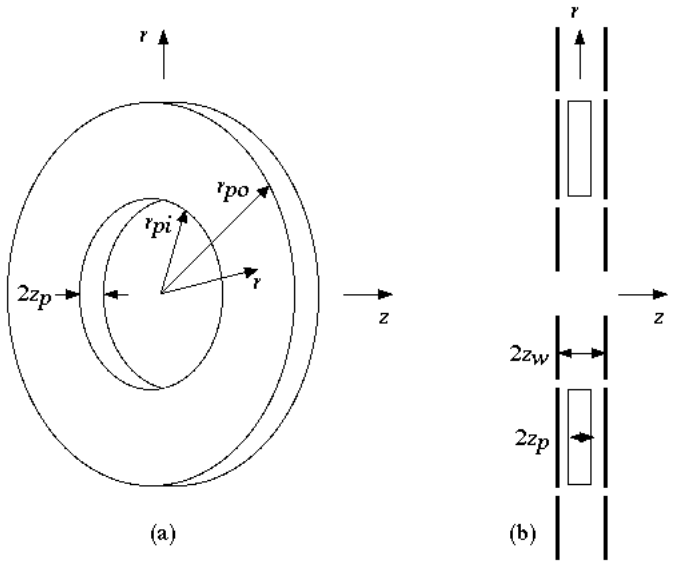

FIG. 5.1. The configuration considered for plasma trapping in a magnetic field given by $\mathbf{B} = B(r)\hat{\mathbf{r}}$. (a) The plasma confined in a washer-shaped region of width z_p extending from $r = r_{pi}$ to $r = r_{po}$. (b) The electrode configuration considered.

Electron confinement with local densities higher than the Brillouin limit using non-thermal electron distributions has also been reported.[5]

The Brillouin Density Limit

Penning traps generally have very good confinement properties. Near perfect axial confinement can be achieved and long term radial confinement is possible in solenoidal fields if the effects of neutral collisions and field imperfections are minimized. However, a nonneutral plasma confined in a Penning trap employing an axial magnetic field has its density limited by the Brillouin density limit.[6] This limit expresses a balance of magnetic, self-electric and centrifugal forces. The electric field on the outer radius of a plasma column is $E(r_p, z) = qnr_p/(2\epsilon_0)$ where r_p is the plasma radius and n is its density. For radial confinement to occur the outwardly directed self-electric and centrifugal forces must be balanced by the magnetic force, $q^2 n r_p/(2\epsilon_0) + m v_\theta^2/r_p = q v_\theta B$. Solving for the plasma density it is found that $n = \epsilon_0 B^2(2\chi - \chi^2)/(2m)$ where $\chi = 2mv_\theta/(qBr_p)$. This density reaches a maximum when $\chi = 1$ which gives the Brillouin limit

$$n_B = \frac{\epsilon_0 B^2}{2m}.$$

This limit can be quite severe in typical magnetic fields. For example the Brillouin limit for a xenon ion plasma in a .2 T magnetic field is $8.1 \times 10^{11}\mathrm{m}^{-3}$.

Studies currently planned involving antihydrogen production or fusion with Penning traps will have reaction rates which strongly depend upon the plasma density. Techniques which allow for confinement in excess of the Brillouin limit could be of substantial interest.[7,8]

Exceeding the Brillouin Limit in a Penning Trap with a Radial Magnetic Field

From Gauss' law an approximation for the axial electric field at any location far from the radial edges of the plasma in the radial configuration can be obtained. The axial component of the electric field within the plasma in this region is $E_z = qnz/\epsilon_0$. The force on a particle due to this electric field, F_E must be balanced by the axially inward magnetic force $F_B = qv_\theta B$. From this balance arises a requirement on the azimuthal velocity, $v_\theta = qnz/(\epsilon_0 B)$. For a plasma in this configuration, the Brillouin limit does not apply because the centrifugal force does not appear in the axial force balance, but a plasma in this radial field configuration necessarily has a sheared rotation. Because of this rotational shear, nearby collections of particles which have different axial locations will exert a torque on each other. This torque will result in axial expansion of the plasma and a finite axial confinement time. However, it may be possible to develop some technique, perhaps similar to a rotating field technique,[9] to keep the plasma from expanding axially. An upper limit on the density which replaces the Brillouin limit for this configuration may be found by examining the axial force balance at $z = z_p$. Setting v_θ equal to the speed of light c, we get the largest possible density in this type of trap

$$n_{max} = \frac{\epsilon_o c B}{q z_p}. \tag{5.1}$$

Considering a 0.2 T magnetic field as before, with a plasma width of 1 cm, we find that $n_{max} = 6.6 \times 10^{17}\,\mathrm{m}^{-3}$.

It should be pointed out that this limiting density is probably considerably larger than that which could easily be produced. However, as this density is several orders of magnitude above the corresponding Brillouin limit, it is possible that a nonneutral plasma could be confined in this form of trap at a density higher than the Brillouin

limit.

In the radial direction, the applied radial electric field must overcome the centrifugal force, the magnetic gradient force, and also the force from the self-electric field of the plasma. The magnetic gradient force on a particle can be evaluated from $\mathbf{F}_M = -\mu\nabla B$ with μ equal to the magnetic moment of the cyclotron orbit of the particle.[10] The magnetic field may be approximated as only having a radial component in the region of the trap containing the plasma so that the condition $\nabla \cdot \mathbf{B} = 0$ implies $B_r = C/r$. The magnetic moment may be approximated as $T_\perp/B$ where $T_\perp$ is the temperature associated with the motion perpendicular to the magnetic field. Hence, $F_M = T_\perp/r$.

The largest value of the centrifugal force which must be overcome by the applied electric field occurs at $z = z_p$. At this location the azimuthal velocity reaches its maximum value of $v_\theta = Zenz_p/(\epsilon_0 B)$.

A self-consistent computation demonstrating an ion plasma confined at a density above the Brillouin limit is shown in Figs. 5.2 and 5.3. The results are generated for singly charged xenon ions with a maximal density of $1.5 \times 10^{13}\,\mathrm{m}^{-3}$ (at $z = 0$, $r = 25\,\mathrm{cm}$) and a temperature of 300 K confined in a trap which extends from $r = 24.5\,\mathrm{cm}$ to $r = 25.5\,\mathrm{cm}$ and from $z = -0.5\,\mathrm{cm}$ to $z = 0.5\,\mathrm{cm}$. Considering the magnitude of the magnetic field to be approximately 0.2 T throughout the region of the trap containing the plasma, the electric field required to balance the maximum centrifugal force evaluates to 250 V/m. The electric field strength required to balance the magnetic gradient force is 0.1 V/m.

For the purpose of the self-consistent calculation, the electrode configuration which is illustrated in Fig. 5.1 is replaced by a series of electrodes which provide

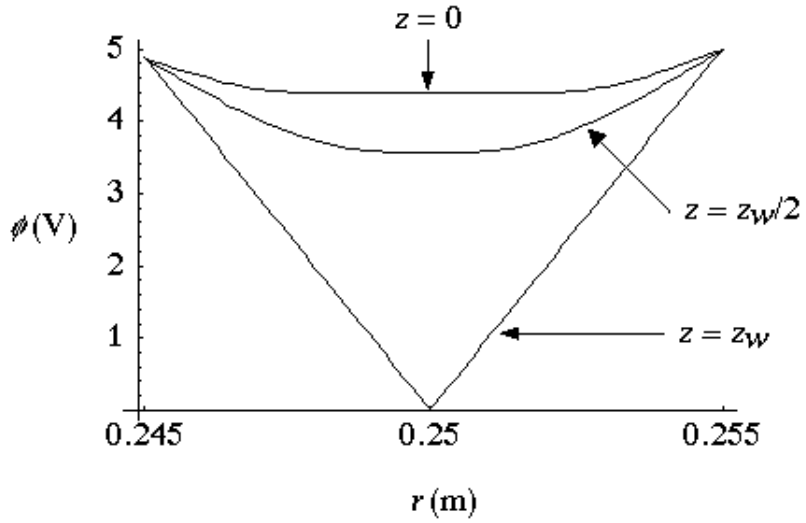

FIG. 5.2. The potential along three different axial lines. The applied potential, along the $z = z_w$ line, is shown along with the self-consistently determined potential along $z = z_w/2$ and $z = 0$.

a triangular potential well. The applied potential linearly decreases from 5 V to 0 V from $r = 24.5\,\mathrm{cm}$ to $r = 25\,\mathrm{cm}$ and then it increases linearly back to 5 V at $r = 25.5\,\mathrm{cm}$. This produces an applied electric field of 1000 V/m. The plasma is assumed to follow the Boltzmann relation along each radial magnetic field line and follow an axial profile along $r = 25\,\mathrm{cm}$ given by $h(z) = 1 - (z/z_w)^\alpha$. The resulting potential is shown in Fig. 5.2. The resulting density is shown in Fig. 5.3.

Because in this configuration the centrifugal force acting on the plasma can be opposed by the force due to an applied electric field instead of a magnetic field, the Brillouin density limit is not applicable. For the 0.2 T magnetic field considered, the ion density considered, $1.5 \times 10^{13}\,\mathrm{m}^{-3}$ is much greater than the Brillouin limit of $8.1 \times 10^{11}\,\mathrm{m}^{-3}$.

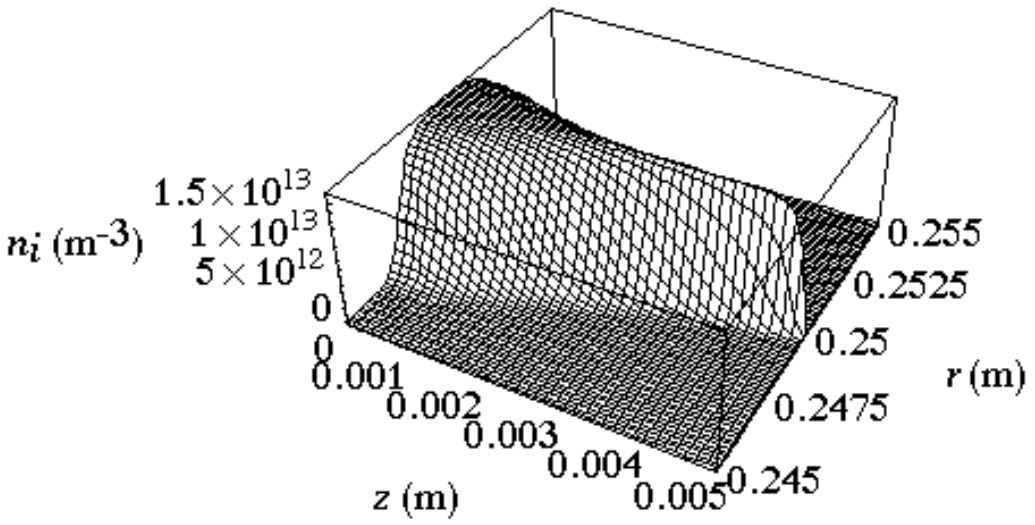

FIG. 5.3. The ion density.

REFERENCES

[1]R. F. Post, "The magnetic mirror approach to fusion," Nucl. Fusion **27**, 1579 (1987).

[2]H. P. Furth, "Existence of mirror machines stable against interchange modes," Phys. Rev. Lett. **11**, 308 (1963).

[3]C. A. Ordonez, "Magnetic cusp and electric nested- or single-well configurations for high density antihydrogen and fusion nonneutral plasma applications," , in *Non-Neutral Plasma Physics III*, edited by J. L. Bollinger, R. L. Spencer, and R. C. Davidson, Melville, New York, 1999, American Institute of Physics.

[4]R. G. Greaves, M. D. Tinkle, and C. M. Surko, "Modes of a pure ion plasma at the Brillouin limit," Phys. Rev. Lett. **74**, 90 (1995).

[5]T. B. Mitchell, M. M. Schauer, and D. C. Barnes, "Observation of spherical focus in an electron Penning trap," Phys. Rev. Lett. **78**, 58 (1997).

[6]L. Brillouin, "A theorem of Larmor and its importance for electrons in magnetic fields," Phys. Rev. **67**, 260 (1945).

[7]R. G. Greaves and C. M. Surko, "Antimatter plasmas and antihydrogen," Phys. Plasmas **4**, 1528 (1997).

[8]D. C. Barnes, T. B. Mitchell, and M. M. Schauer, "Beyond the Brillouin limit with the Penning fusion experiment," Phys. Plasmas **4**, 1745 (1997).

[9]F. Anderegg, E. M. Hollman, and C. F. Driscoll, "Rotating field confinement of pure electron plasmas using Trivelpiece-Gould modes," Phys. Rev. Lett. **81**, 4875 (1998).

[10]G. Schmidt, *Physics of High Temperature Plasmas*, Academic Press, New York, 1979.

CHAPTER 6

ANTIHYDROGEN PRODUCTION USING A NESTED WELL PLASMA TRAP

An area of current research interest is the production of well-confined low temperature antimatter in the form of antihydrogen. In 1996 the production of a small number of antihydrogen atoms was reported.[1] This was accomplished via a reaction of an antiproton with an atomic nucleus in which a positron is produced and captured by the antiproton. However, only on the order of 10 antihydrogen atoms were produced and these were produced at a high kinetic energy.

The CERN AD (Antiproton Decelerator) facility will allow for a variety of experiments aimed at producing and confining antihydrogen atoms. Of particular interest will be studies of the spectrum of antihydrogen and comparison to that of hydrogen.[2] Experiments of this type will make possible very precise tests of CPT invariance.[3] Additionally, there is interest in measuring the gravitational acceleration of antimatter, thereby testing the weak equivalence principle. Such tests are extremely difficult to perform for charged particles due to the difficulty of shielding out electromagnetic forces. The production of cold antihydrogen should make these experiments feasible.[2]

One method of low temperature antihydrogen production which has been proposed is to confine both antiproton and positron plasmas in a nested well Penning trap so that they have a significant region of overlap.[4–6] As has been discussed in Chap. 2 there are two methods by which two plasmas of equal charge magnitude but opposite sign may be confined together in such a trap with a region of signifi-

cant overlap. One method requires that the two plasmas have a large temperature difference. The hotter component would reside primarily within the end wells but have a high enough temperature that it can overcome the potential hill between the outer and inner well and will overlap the inner well significantly.

Alternately, an overlap of the two plasmas may be achieved by keeping the outer well plasma in a nonequilibrium state. In particular, the nonequilibrium state used is the "antishielding state" in which the outer well plasma particles pass through the outer wells with enough momentum to carry them into the inner well. The antishielding state can be prepared such that within the inner well this component will approximately have a Maxwellian velocity distribution with a low (<1 K) temperature. Collisions, or possibly microinstabillities, will cause this distribution to relax towards equilibrium. As this relaxation occurs the two components will separate. To ensure that a significant amount of antihydrogen can be produced before the two components separate it is necessary to select the trap parameters such that the timescale for antihydrogen recombination is much smaller than the timescale for relaxation of the plasmas. Alternately, a time-dependent procedure may be implemented that re-establishes the antishielding state many times.

Regardless of the method used to achieve overlap, the overlap region may be prepared such that it is either neutral or nonneutral. Use of a nonneutral overlap would create an electric field within the inner well region. Depending on the magnitude of the charge imbalance, this field could cause the re-ionization of newly created antihydrogen atoms which would initially be in highly excited states. Within this chapter, several methods of achieving overlap, antihydrogen recombination and trapping are considered. A neutral overlap region achieved with equal temperature

positron and antiproton plasmas is identified as the most favorable for antihydrogen recombination and trapping. Effects which may occur in a nonneutral overlap region are also considered, and parameter ranges in which the effects may be important are predicted.

Antihydrogen Production From Components With Disparate Temperatures

To use a Penning trap for antihydrogen recombination requires confining two oppositely charged plasma components in the same spatial region. For the case in which both plasma components are in thermal equilibrium two conditions on the voltage difference between the inner well and outer well apply. Assuming antiprotons are the inner well species, the condition for them to have adequate axial confinement is $e\Delta\phi_m/T_- \gg 1$ where $\Delta\phi_m$ is the difference in potential from the $z = 0$ to the axial location where the potential reaches its minimum value along a magnetic field line. In other words, $\Delta\phi_m$ is the inner well depth along a magnetic field line. The second condition is $e\Delta\phi_m/T_+ \lesssim 1$. This condition is necessary to allow the positrons, which are primarily confined within the outer well, to have a significant overlap of the inner well. Both of these conditions may be met with thermally relaxed plasmas only if $T_- \ll T_+$.

To confine the antihydrogen produced in a superimposed magnetic minimum requires that the antihydrogen be produced at temperatures of no more than 1 K so that the antihydrogen atoms can be confined as a result of their permanent magnetic dipole moment. Trapping of 1 K antihydrogen in a Ioffe-Pritchard magnetic field configuration may be possible.[2] Such a system is azimuthally asymmetric, and experimental studies are now underway to study the effect of this asymmetry on a superimposed Penning trap.[7] The possibility of using a magnetic cusp configuration

which has azimuthal symmetry also exists. An Andreoletti-Furth configuration is symmetric about the axis[8] and is being investigated for antihydrogen confinement. The magnetic minimum in either the Ioffe-Pritchard or Andreoletti-Furth configuration could be arranged to occur in the overlap region of a nested well trap and allow for the trapping and de-excitation of newly-formed antihydrogen.

Because of the requirement that the antihydrogen be produced at no more than approximately 1 K, the antiproton component, must have a temperature of less than 1 K. If the antiprotons are the inner well species, as is assumed here, the positrons must have a temperature much higher than 1 K. If the role of the two plasma components is reversed and the positrons are held in the inner well, the positron temperature must be significantly less than 1 K. For this reason the situation where the antiprotons are the inner well species is much more feasible. However, there is an additional difficulty with using the two-temperature approach to achieve antihydrogen recombination. The recombination rate decreases significantly as positron temperature increases.[4] So a very low positron temperature is also desirable.

Antihydrogen Production Using a Nonequilibrium Plasma

Establishment of a nonequilibrium "antishielding" distribution in one dimension is discussed in Chap 2. Essentially the antishielding state is established by initially confining a plasma component outside of the nested well trap at a potential equal to that inside the inner well. Because the nonequilibrium state is predicted to have a longer persistence for a higher mass component (see below), we will assume that the positrons are the species confined within the inner well and that antiprotons are the outer well species, although the roles of the two plasma components could be reversed.

While the two components are separated, the positron plasma is allowed to cool via synchrotron radiation to the temperature of the surrounding structure. This occurs with a timescale of less than a second for large magnetic fields ($B > 2\,T$).[6] To cool the antiprotons, electrons may be confined in the same well. After cooling has occurred, the electrons may be selectively removed.[9]

After both positron and antiproton plasmas are prepared in a 1 K thermal equilibrium state, the potential barriers keeping the antiproton plasma out of the nested well are removed, allowing this component to flow into the nested well as demonstrated in Fig. 2.4. After the antiprotons flow into the nested well, their axial density profile is given by

$$n_- = n_{0-} e^{\psi_-} \mathrm{erfc}\left[\mathrm{Re}(\sqrt{\psi_-})\right] \tag{6.1}$$

where n_{0-} is the density at $z = 0$, $\psi_- = e\left[\phi(z) - \phi_0\right]/T_-$ is the electric potential normalized to the antiproton temperature, and ϕ_0 is the potential at $z = 0$. This density profile applies to a collisonless Maxwellian plasma that is allowed to flow into an initially empty well so that it flows through the well without becoming trapped. Because the axial speed of the plasma is greater within the well, the plasma will, by conservation of flux, have a smaller density within the well than outside of it. Therefore, a nonneutral plasma which follows Eq. 6.1 will increase the depth of, or "antishield," the well. Because $\phi(z)$ in the inner well region is chosen to be equal to ϕ_0, the velocity distribution of the antiprotons in the inner well just after they have been allowed to enter the nested well is Maxwellian with an associated temperature equal to the plasma's temperature before it enters the nested well. By this method, both plasmas may have temperatures less than 1 K within the inner well. The average relative speed between positrons and antiprotons can be low, and

consequently their recombination rate can be high.

CERN AD will be capable of producing only a limited number of antiprotons, and the density of the plasmas considered for these experiments will be low. Experiments have been reported in which around 10^5 antiprotons have been accumulated.[10,11] The facilities at CERN produce on the order of 10^7 antiprotons per pulse.[12] For the trap considered in this section, an antiproton density of around 10^9 to $10^{10}\,\mathrm{m}^{-3}$ is expected. For plasmas of this density, the magnitude of the change in potential from $r = 0$ to $r = r_w$ will be only on the order of a few millivolts. However, in comparison to the thermal energy of the 1 K ($8.7\times10^{-5}\,\mathrm{eV}$) antiprotons, this change in potential can be very important.

In consideration of the form of the two-dimensional potential, it becomes evident that some modification to the procedure for establishing the antishielding state is necessary. As the potential of neither the initial antiproton well or positron well will be radially flat, the one dimensional scheme for achieving overlap that is depicted in Fig. 2.4 can be achieved exactly at only one radial position at best. The effect of having an unneutralized plasma within each initial well is that the positron well will have a higher potential at $r = 0$ than at $r = r_w$; the antiproton well will have a lower potential at $r = 0$ than at $r = r_w$. But by manipulating the applied voltages, the potential difference between the two wells can be arranged to be exactly equal at some radius. For all other radii, the antiprotons will either lose or gain kinetic energy upon moving from their initial well into the inner well if they remain at the same radial position. Depending on the parameters chosen, antiprotons may lack energy to enter the inner well at many radial positions.

Alternate procedures for establishing a nonequilibrium distribution could be de-

vised. Consider the procedure shown in Fig. 6.1. This procedure is implemented using a series of seven cylindrical electrodes. In essence these electrodes create a set of three nested electric potential wells. As shown in Fig. 6.1(a) the innermost well initially confines a 1 K antiproton plasma, and the intermediate well initially confines 1 K positrons. The outermost well is biased positive and initially is empty. Because the two plasmas are at the same temperature, the initial amount of overlap will be negligible.

Once the configuration in Fig. 6.1(a) is achieved, the innermost well potential can be dropped as shown in Fig. 6.1(b), creating the typical nested well profile. Within the new inner well, the positron plasma will adjust to the change in potential before the antiproton plasma moves appreciably. The positrons will spread throughout the inner well and recombination may begin. In this procedure, as before, neither the initial antiproton or positron region will have a radially flat potential. It is expected, therefore, that for many radial positions a significant amount of energy will be gained by the positrons.

Once the antiprotons begin to flow out of the inner well, they will reflect within the end wells and return to the inner well with the same kinetic energy with which they left, provided they do not move radially very far from their starting point. The antiprotons will very precisely match a 1 K Maxwellian velocity distribution within the inner well at all radial values. Because the positrons should thermalize and cool rapidly, this procedure is expected to be more favorable for recombination than the procedure in Fig. 2.4, which will set up two opposing antiproton beams in the inner well at most radial positions.

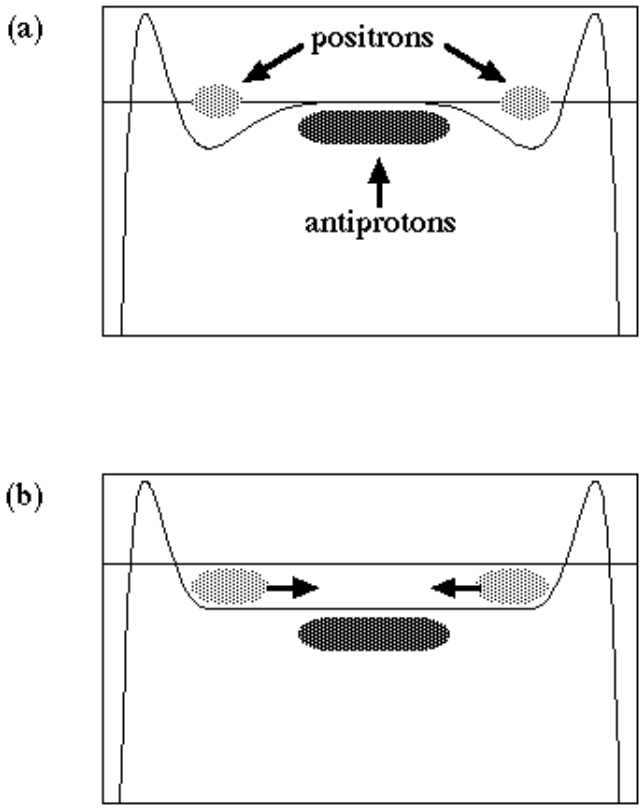

FIG. 6.1. Illustration of an alternate process for loading an antiproton plasma into nested electric potential wells such that the antiproton plasma will overlap a positron plasma. This procedure allows the antiprotons to enter into the desired nonequilibrium state at all radial locations. The initial profile (a) has three nested electric potential wells. The innermost contains an antiproton plasma. The intermediate well contains a positron plasma which does not overlap the inner well. The outer-most well is empty. By quickly adjusting the applied potential of the center electrode, a typical nested well potential profile is generated (b). The positrons diffuse into the new inner well rapidly. The antiprotons enter the end wells.

Calculation of the Timescale for Antiproton Recombination

The evolution of the plasmas within the nested well trap can be characterized by two timescales: τ_r, the timescale for recombination of positrons and antiprotons to form antihydrogen, and τ_s, the separation timescale which is characteristic of the rate at which the antiproton and positron plasmas separate due to the relaxation of the antiproton plasma.

Two mechanisms by which antihydrogen can be produced are considered: three-body recombination and radiative recombination.[4,13] Holzscheiter gives the spontaneous radiative recombination reaction rate as $\alpha^{SRR} = 9 \times 10^{-17} \mathrm{m}^3\,\mathrm{s}^{-1}$ for 0.1 meV($\approx$ 1K) positron and antiproton plasmas.[2] From this reaction rate the recombination timescale can be calculated as $\tau^{SRR} = 1/(\alpha^{SRR} n_+)$. Typically, we will be considering plasmas with $n_+ \approx 10^{10}\,\mathrm{m}^{-3}$. For such a plasma, $\tau^{SRR} \approx 10^6\,\mathrm{s}$.

Three-body recombination is a process by which a positron and antiproton recombine and a second positron nearby carries off excess energy and momentum. This reaction becomes more important as the positron density increases. The three-body recombination reaction rate for antihydrogen in the absence of a magnetic field is[4]

$$\alpha^{TBR} = 6 \times 10^{-24} (4.2/T)^{9/2} n_+.$$

Magnetic fields will have a detrimental effect on the recombination rate. However, even in an infinitely large magnetic field the rate will only be less by an order of magnitude.[14] The timescale for this reaction, including the effect of a large magnetic field $\tau^{TBR} = 10/(\alpha^{TBR} n_+)$. For a 1K mixture of positrons and antiprotons with $n_+ = 10^{10}\,\mathrm{m}^{-3}$, $\tau^{TBR} = 30$ s. Clearly for the plasmas considered in this section three-body recombination is expected to be the dominant recombination process.

Calculation of the Timescale for Relaxation of the Antishielding Distribution to Equilibrium

Another timescale relevant to the use of a nested well trap for production of antihydrogen is the timescale for the process by which antiprotons in the antishielding state leave the inner well region and become trapped in the end wells. This process must occur at a much slower rate than the antihydrogen recombination process for a significant amount of antihydrogen to be produced without requiring a time dependent manipulation of the electrode potentials to reset the antishielding distribution.

The timescale for the relaxation of the antishielding distribution, τ_s, can be calculated by $\tau_s = N_i/\dot{N}_o$, where N_i is the number of antiprotons in the inner well and $\dot{N}_o$ is the rate at which the antiprotons become trapped in the outer well. Rewriting in terms of the antiproton density in the inner well, n_i, the cross sectional area of the trap, A, the length of the inner well, L, and the flux into each end well, F, we obtain

$$\tau_s = n_i L/(2FP_t) \tag{6.2}$$

where P_t is the probability that an antiproton which enters the inner well will become trapped there.

Within the inner well (where $\psi = 0$) the antiprotons will have a Maxwellian velocity distribution. The flux associated with particles with a Maxwellian velocity distribution is

$$F = \frac{n\mathrm{e}^{-\psi}}{\sqrt{2\pi m/T}}.$$

Evaluating this flux at the edge of the inner well ($\psi = 0$, $n = n_i$) and substituting

into Eq.6.2 yields

$$\tau_s = \frac{L\sqrt{\pi m/(2T)}}{P_t}.$$

If there are no collisions, all the antiprotons that enter the end well will be reflected at the ends of the trap, and re-enter the inner well with the same energy with which they left; P_t will equal zero and the antishielding state will persist forever. However, collisions do occur, and a model for the trapping probability is[15]

$$P_t = \mathrm{erf}\left(\sqrt{\langle \Delta\epsilon_x \rangle / T}\right)$$

where

$$\langle \Delta\epsilon_x \rangle = \frac{L_m \mathrm{e}^4 n_+ \left[\mathrm{e}^{\psi_m}\mathrm{erfc}\left(\sqrt{\psi_m}\right)\right]^3 \lambda}{128\epsilon_0^2 T},$$

and

$$\lambda = \frac{1}{2}\ln\left(1 + \frac{256 m \epsilon_0^2 T^3}{e^6 B^2 \left[\mathrm{e}^{\psi_m}\mathrm{erfc}\left(\sqrt{\psi_m}\right)\right]^4}\right)$$

is the Coulomb logarithm. Here $\psi_m = e\Delta\phi_m/T_-$ and L_m is the length of the end well plasma. The equation for the timescale of the persistence of the antishielding state, τ_s, is of the same form regardless of whether positrons or antiprotons are the outer well species. However, antiprotons will have the longer timescale because of their larger mass.

For the parameters given in Table 6.1, the self-consistently calculated depth of the end well is $\Delta\phi_m = 1.4$ V. Using this value and the other parameters given in Table 6.1 results in $\tau_r = 0.6$ s and $\tau_s = 38$ s. Because τ_s is so much larger than τ_r most of the antiprotons are expected to recombine before their distribution relaxes towards equilibrium, and they become trapped in the end wells.

Recombination and Trapping Considerations

In principle the system may be prepared such that the inner well region is neutral or nonneutral. Within a nonneutral region, the radial electric field may cause the re-ionization of newly created antihydrogen. Additionally, in a nonneutral region both of the plasma components will rotate, and due to the mass difference between the components, each species will have a different rotation rate. Assuming this does not cause an instability to occur, collisions will cause a torque to be applied between the components, and radial separation may occur.

A large disparity in rotation rates may also result in an average relative speed between the plasma species larger than that associated with the thermal motion of the particles. If this occurs, the recombination rate may be reduced.

For overlapping antiproton and positron plasmas of constant densities n_- and n_+, the rotation rates will be

$$\omega_{r+} = \frac{\omega_{c+}}{2}\left(1 \pm \sqrt{1 - \frac{2\omega_{p+}^2}{\omega_{c+}^2}}\right)$$

for the positrons, and

$$\omega_{r-} = \frac{\omega_{c-}}{2}\left(1 \pm \sqrt{1 + \frac{2\omega_{p-}^2}{\omega_{c-}^2}}\right)$$

for the antiprotons, where $\omega_{c\pm} = qB/m_\pm$, $\omega_{p\pm} = \sqrt{(q^2\Delta n)/(\epsilon_0 m_\pm)}$, $\Delta n = n_+ - n_-$ and $m_\pm$ is the positron (antiproton) mass. Choosing the negative sign in the expression for the antiproton rotation rate gives a rotation in the same direction as the positrons. Choosing the slow rotation rate for the positrons will give the smallest difference in rotation rates. Figure 6.2 shows the difference in azimuthal velocity that occurs at $r = r_w$ in comparison to each plasma component's thermal speed, $v_T = \sqrt{T/m}$ (considering a temperature of 1 K) for various values of $\Delta n =$

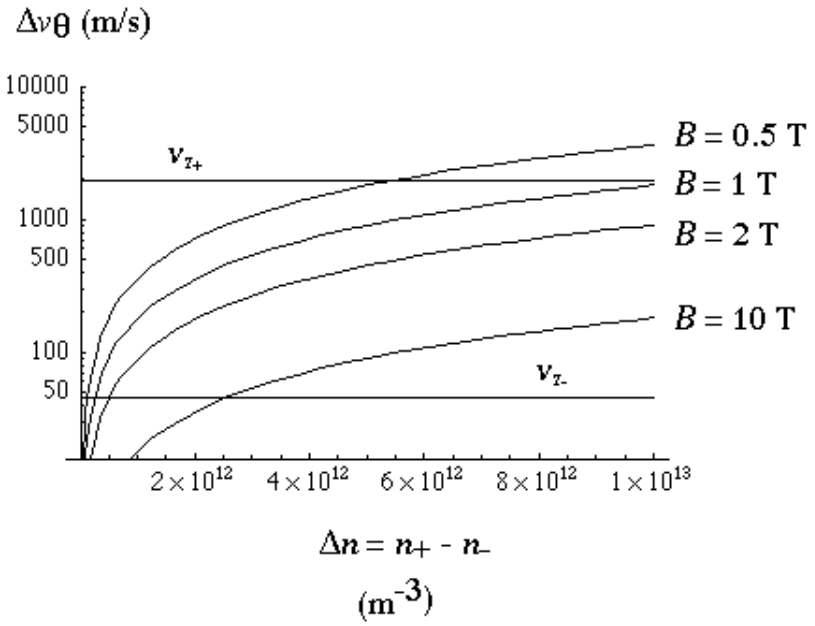

FIG. 6.2. The difference in rotational velocity, Δv_θ at $r = r_w = 5\,\mathrm{cm}$ for positrons and antiprotons in various magnetic fields versus Δn. Also shown are the thermal velocities of the positrons, v_{T+}, and antiprotons, v_{T-}. As Δv_θ becomes appreciable compared to the thermal velocities, the recombination rate may be affected.

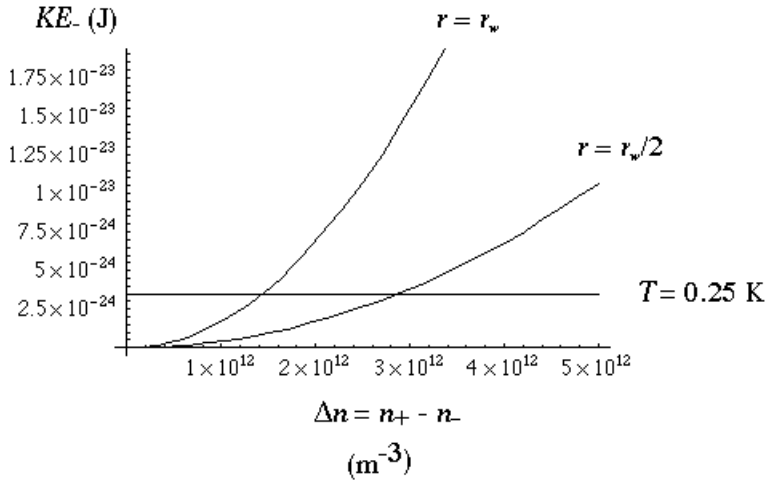

FIG. 6.3. The kinetic energy associated with the azimuthal velocity of the antiprotons at $r = r_w$ and $r = r_w/2$.

$n_+ - n_-$. For a magnetic field of 2 T which is considered in this chapter, the effects on the recombination rate associated with a disparate rotation rate will only become important when Δv_θ approaches the speed of the positrons.

Additionally, for a nonneutral overlap region, the kinetic energy associated with the antiproton rotation can be larger than the antiproton thermal energy. Even if recombination occurs, the rotational kinetic energy of the antiprotons may make trapping of the antihydrogen atoms impossible. The kinetic energy associated with antiproton rotation at both $r = r_w$ and $r = r_w/2$ is shown versus Δn in Fig. 6.3. It can be seen that the antiproton rotational kinetic energy becomes appreciable for $\Delta n \approx 2 \times 10^{12}\mathrm{m}^{-3}$ or larger.

Self-Consistent Calculation of Trap Properties

A self-consistent calculation has been performed using the SOR code described in Chap. 2 and presented in Appendix B. The simulation determines the particle distributions and potential self-consistently immediately after the antishielding state

Table 6.1. Parameter values used for the calculation of the electric potential and plasma density distributions in a nested well plasma trap confining positrons and antiprotons for the purpose of producing cold antihydrogen.

Parameter	**Value**
r_w	1 cm
L_0	24 cm
L_1	2 cm
L_2	1 cm
V_1	1.5 V
V_2	-0.4 V
$n_+(0,0)$	3×10^9 m^{-3}
$n_-(0,0)$	3×10^9 m^{-3}
B	2 T
T_-/k	.25 K
T_+/k	.25 K

is established.

For the purposes of the calculation, the density distribution of the antiprotons is described by Eq. 6.1 along each magnetic field line, while the positrons follow the Boltzmann relation within the inner well along each field line. The radial profile of each component is selected to be parabolic in form and drops to zero at $r = r_w/2$. Other values used in the computation are given in Table 6.1. The outer electrode is given a length equal to the trap radius, $L_2 = r_w$. Additionally, the trap is closed by an electrode cap at the end of the outer electrode that is held at voltage V_2 for the purposes of the computation. This is done for computational ease. The results generated are expected to apply to a corresponding open-ended trap with a much larger value of L_2. The voltages chosen will be large enough compared to the plasma temperature to provide very good confinement of both plasma species. The results of the calculation are shown in Fig. 6.4. The on-axis potential is shown in Fig. 6.4(a). The on-axis antiproton and positron densities are shown in Fig. 6.4(b)-(c). The

peaks in the antiproton density occur at axial locations where $\phi(z)$ exactly equals ϕ_0. The results show neutrality throughout the inner well region, which should allow recombination to occur without the possibility of ionization by electric fields.

Summary

In this chapter an analysis of the use of a nested well Penning trap for antihydrogen recombination is presented. The possibility of using plasma components with different temperatures is discussed, but a scenario in which equal temperature antiproton and positron plasmas are made to overlap such that a neutral inner well region is obtained is identified as most favorable for antihydrogen recombination and trapping. Obtaining this overlap requires the use of a nonequilibrium distribution for one plasma component. A method which should allow the nonequilibrium "antishielding" state to approximately be achieved at all radial locations is presented. Additionally, expressions for the timescales for both antihydrogen production and relaxation of the antishielding state to equilibrium are developed.

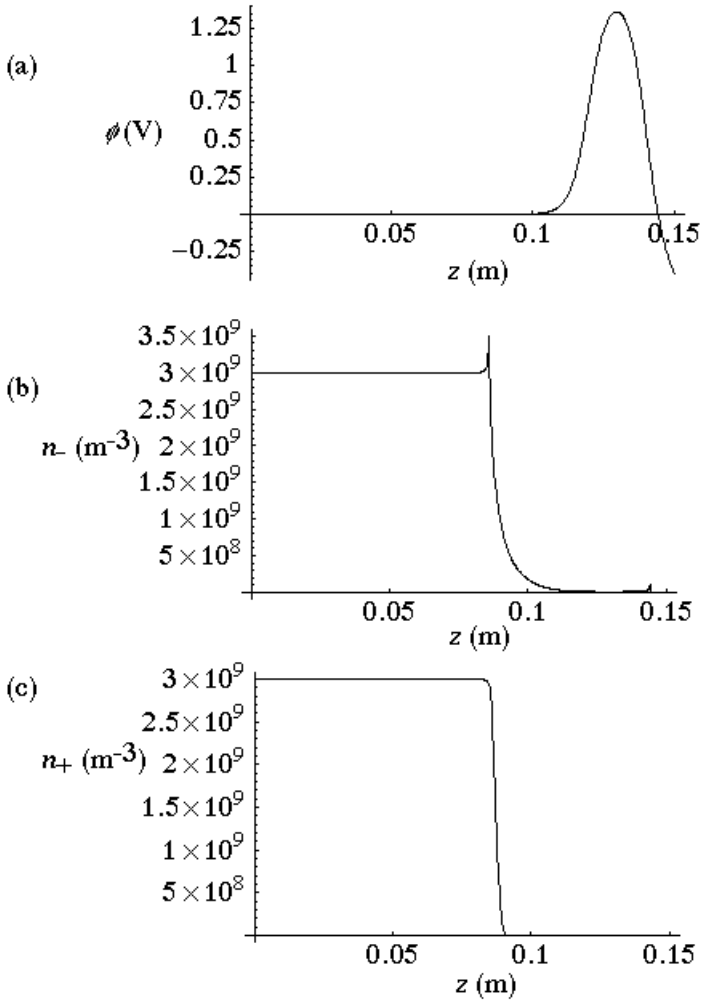

FIG. 6.4. The self-consistent electric potential (a), antiproton density (b), and positron density (c) along the axis of a nested Penning trap under conditions suitable for antihydrogen recombination and trapping. The profiles are symmetric about the midplane (at $z = 0$), and only the profiles for $z > 0$ are computed. A uniform magnetic field parallel to the z axis is assumed.

REFERENCES

[1]G. Baur, "Production of antihydrogen," Phys. Lett. B **368**, 251 (1996).

[2]M. H. Holzscheiter and M. Charlton, "Ultra-low energy antihydrogen," Rep. Prog. Phys. **62**, 1 (1999).

[3]R. Bluhm, V. A. Kostelecky, and N. Russell, "CPT and Lorentz tests in hydrogen and antihydrogen," Phys. Rev. Lett. **82**, 2254 (1999).

[4]G. Gabrielse, S. l. Rolston, L. Haarsma, and W. Kells, "Antihydrogen production using trapped plasmas," Phys. Lett. A **129**, 38 (1988).

[5]J. Eades and F. J. Hartmann, "Forty years of antiprotons," Rev. Mod. Phys. **71**, 373 (1999).

[6]R. G. Greaves and C. M. Surko, "Antimatter plasmas and antihydrogen," Phys. Plasmas **4**, 1528 (1997).

[7]E. Gilson and J. Fajans, "Quadrupole induced resonant particle transport in a pure electron plasma," , in *Non-Neutral Plasma Physics III*, edited by J. L. Bollinger, R. L. Spencer, and R. C. Davidson, Melville, New York, 1999, American Institute of Physics.

[8]R. F. Post, "The magnetic mirror approach to fusion," Nucl. Fusion **27**, 1579 (1987).

[9]G. Gabrielse et al., "The ingredients of cold antihydrogen simultaneous confinement of antiprotons and positrons at 4 K," Phys. Lett. B **455**, 311 (1999).

[10]P. O. Fedichev, "Formation of antihydrogen atoms in an ultra-cold positron-antiproton plasma," Phys. Lett. A **226**, 289 (1997).

[11]G.Gabrielse et al., "First capture of antiprotons in a Penning trap: A kiloelectronvolt source," Phys. Rev. Lett. **57**, 2504 (1986).

[12]D. Möhl, "Production of low-energy antiprotons," Hyperfine Interactions **109**, 33 (1997).

[13]Y. Chang, D. D. Dolliver, and C. A. Ordonez, "Analysis of time-dependant effects when operating nested-well plasma traps for achieving antihydrogen recombination," , in *Non-Neutral Plasma Physics III*, edited by J. L. Bollinger, R. L. Spencer, and R. C. Davidson, Melville, New York, 1999, American Institute of Physics.

[14]M. E. Glinsky and T. M. O'Neil, "Guiding center atoms: Three body recombination in a strongly magnetized plasma," Phys. Fluids B. **3**, 1279 (1991).

[15]C. A. Ordonez, "Time-dependent nested-well plasma trap," IEEE Trans. on Plasma Sci. **24**, 1378 (1996).

[16]G. Baur et al., "Search for antihydrogen at LEAR," Phys. At. Nuclei **59**, 1509 (1996).

[17]R. J. Goldston and P. H. Rutherford, *Introduction to Plasma Physics*, Institute of Physics Publishing, Philadelphia, 1995.

APPENDIX A

SOR CONVERGENCE TESTING AND ACCURACY

The use of a relaxation method technique requires that some testing be done to determine if the solution has been approached to the desired precision. The method by which this is achieved involves calculating the change in ϕ at each grid point during each computational step,

$$\zeta_{i,j} = \phi_{i,j}^{n+1} - \phi_{i,j}^{n}.$$

Then by summing up $|\zeta|$, or alternately ζ^2, over all grid points, a sum known as the residual is generated. Typically the SOR method is characterized by an initial divergence or slow convergence for several timesteps, depending on the initial choice used for ϕ. During this time the residual grows. After this initial divergence, however, the solution rapidly and steadily converges for most problems if a solution may be found. Typical behavior of the residual is shown in Fig. A.1 both when a solution is reached (a) and when a solution is not found (b).

For comparison, a graph of the residual per time step is shown in Fig. A.2 for a simple relaxation method solution (setting $\omega = 1$ in Eq. 2.1). The same parameters where used in the calculation of both Fig. A.1(a) and Fig. A.2.

Accuracy of the SOR solutions

The accuracy of the SOR calculation depends upon the number of grid points used as well as the ratio of plasma Debye length and grid spacing. As the Debye length is the scale length over which the plasma and the potential change appreciably, the computational grid spacing needs to be smaller than this to accurately represent the plasma. Spencer gives a requirement of two grid points per Debye length for accuracy within 1%.[1]

As a test of the method's accuracy, consider a long trap filled with a plasma that follows a fixed, parabolic radial profile, $h(r) = 1 - (r/r_w)^2$. If the plasma column is

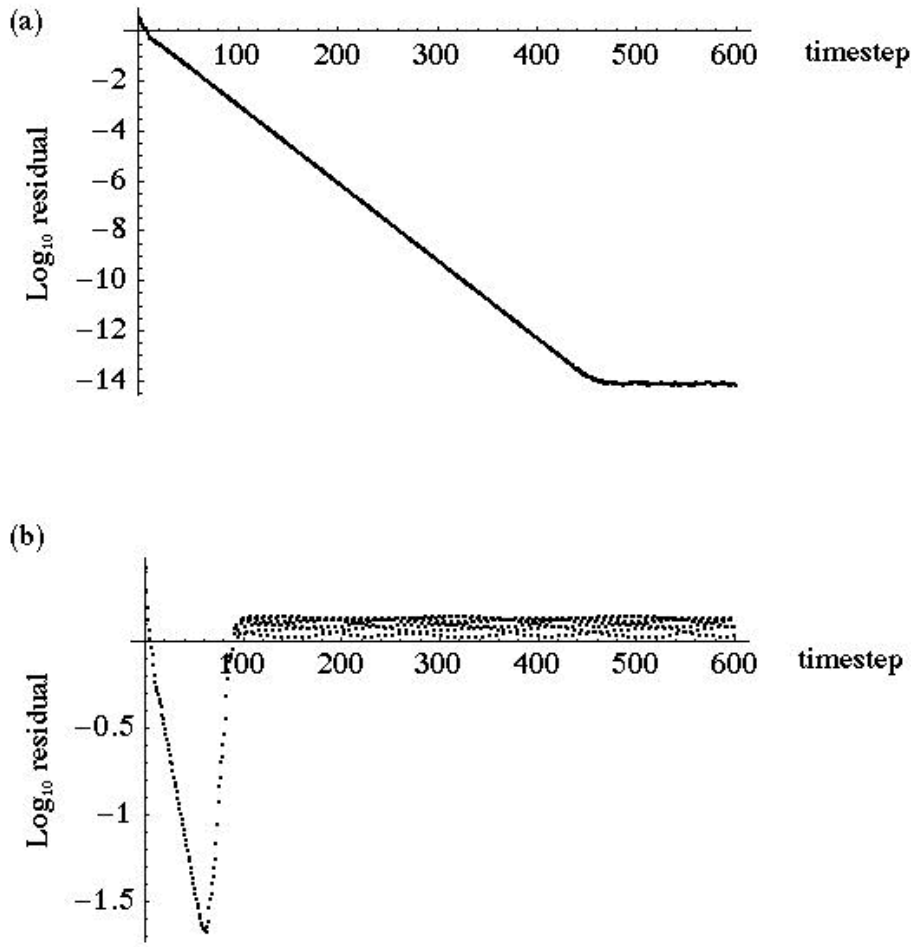

FIG. A.1. The residual versus timestep for a typical SOR solution (a). This demonstrates convergence down to the precision available. Also shown is the residual versus timestep for a non-convergent problem (b). In this case the plasma density used was to great for the applied voltages, and no solution was found

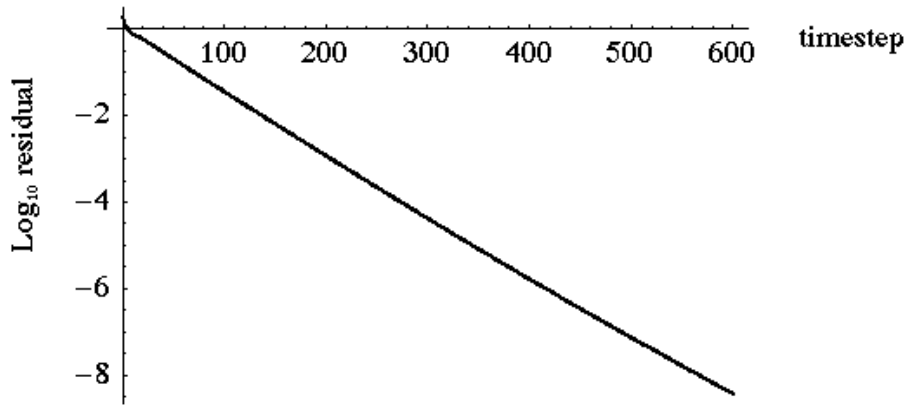

FIG. A.2. The residual generated by solving the same problem used in Fig. A.1(a) by a simple relaxation method. While the SOR calculation had converged to the precision available ($\approx 10^{-14}$) by timestep 450, the simple relaxation method has only achieved a change of around 10^{-8} per timestep by the end of the run.

long enough that fringing fields from the confining electrode are not important then the potential at the midplane may be compared to the exact result for an infinite length plasma column with that radial profile,

$$\phi(r) = -\frac{n_0 q}{\epsilon_0}\left(\frac{r^2}{4} - \frac{r^4}{16 r_w^2}\right) + \phi_0$$

where n_0 is the plasma density at the origin, q is its charge, and r_w is the trap radius, and ϕ_0 is a constant used to match the boundary condition at $r = r_w$. The computational trap used for these accuracy tests had a length twenty times its radius. Therefore, the infinite length expression should be an adequate test.

The results of this accuracy test show a strong dependence on the number of grid points used. Results with 20, 10, and 5 radial grid points were run. Each was allowed to fully converge. The potential for the 5 grid point run was off by 10.9% at $r = 0$. The 10 grid point run was off by 2.8% at $r = 0$ while the 20 grid point

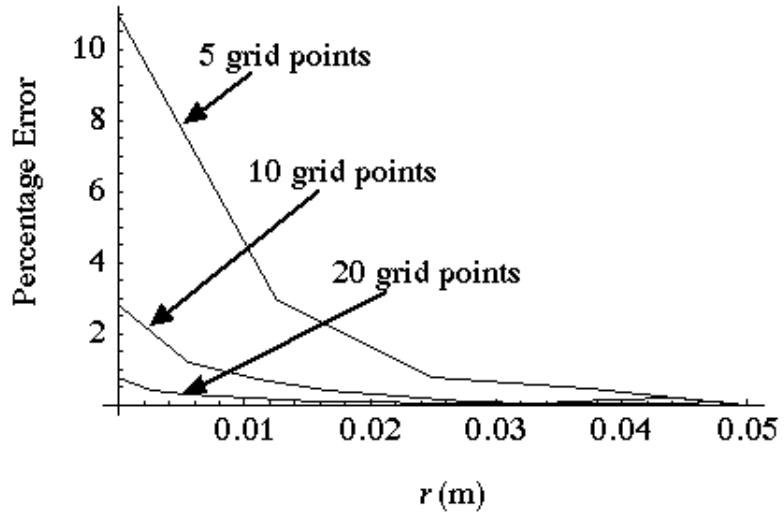

FIG. A.3. The percentage error at each radial location for 5, 10, and 20 grid point solutions.

trial was only off by 0.7%. These results are shown in Fig. A.3. Note that all results were most in error at $r = 0$. A large portion of this error, particularly for the small grid sizes, is a systematic error. Furthermore, this error is not inherent within the SOR method itself but rather is dependent on the way computational boundary conditions are enforced.

In particular, this error comes about by enforcing the symmetry condition at $r = 0$. At $r = 0$, the condition $\frac{\partial \phi}{\partial r} = 0$ applies. A simple way to enforce this is to finite difference the symmetry condition and therefore set

$$\phi_{1,j} = \phi_{2,j} \tag{A.1}$$

where $\phi_{i,j}$ is the potential at radial grid point i, axial grid point j. However, in doing so we have made a condition which should apply at only one point $r = 0$,

apply throughout the entire first radial cell. For fine enough grids this distinction is unimportant. While all results in previous chapters set the $r = 0$ boundary in this manner, all grids used to produce the results throughout this work used more than twenty grid points, so the error from this source should be less than 1% at all grid points. It should also be noted that within a neutral region, the condition $\phi_{1,j} = \phi_{2,j}$ is exact. However, more accurate determinations of the potential along $r = 0$ could be devised and should lead to greater accuracy for the first few radial grid points for solutions calculated with few grid points.

One possibility is to consider the entire first radial cell to be filled with a plasma of constant density $n_{1,j}$,the self-consistent plasma density at $r = 0$. If this approximation is made, we may treat the first cell as a cylinder of charge and apply Gauss' Law to determine the field and change in potential. The relationship between the potential at $r = 0$ and $r = \Delta r$ ($i = 1$ and $i = 2$) becomes

$$\phi_{1,j} = \phi_{2,j} + \frac{q n_{1,j}}{4\epsilon_0} \Delta r^2. \tag{A.2}$$

This produces a significantly improved accuracy for a small grid size problem compared with A.1. For a 5 grid point run, this produces an accuracy everywhere within 3%. For larger numbers of grid points, this method remains more accurate, but the difference between the two methods becomes much less important.

REFERENCES

[1]R. L. Spencer, S. N. Rasband, and R. R. Vanfleet, "Numerical calculation of axisymmetric non-neutral plasma equilibria," Phys. Fluids B **5**, 4267 (1993).

APPENDIX B

SOR CODE

```
(*The Mathematica code used to self - consistently calculate potential and particle
distributions for nested  well plasma traps*)
(*Initialization*)
(*note : MKS units unless otherwise noted.*)
(*physical constants*)
q0 = 1.60218*10^-19;
ϵ0 = 8.85419*10^-12;
(*trap parameters*)
(*radius of the cylindrical electrodes*)
rw = .010;
(*axial position of end of the last electrode (half length of trap)*)
zw = .15;
(*start of potential step*)
z1 = .12;
(*end of potential step*)
z3 = .14;
(*step electrode voltage*)
v2 = 1.5;
(*end voltage*)
v4 = -.4;
(*plasma parameters*)
(* central plasma densities (at (r, z) = (0, 0)*)
n0pos = 3*10^9;
n0neg = 3*10^9;
```

(*temperature of each plasma component in K*)

tKneg = 1000;

tKpos = 1000;

(* starting potential for antishielding distribution*)

ϕ0 = 0;

(*convert to β in 1/joules*)

tneg = tKneg*8.696*10^-5*q0;

tpos = tKpos*8.696*10^-5*q0;

βpos = 1/tpos;

βneg = 1/tneg;

(*Determine Debye length and mimimum grid size needed for 1% accuracy*)

λD = ((ϵ0 tneg tpos)/(tpos n0neg q0^2 + tneg n0pos q0^2))^(1/2)

imin = rw/λD*2

jmin = zw/λD*2

(*computational parameters*)

(*number of grid points in r*)

imax = 20;

(*number of grid point in z*)

jmax=100;

immo = imax - 1;

jmmo = jmax - 1;

(*grid spacing*)

Δr = rw/(imax - 1);

Δz = zw/(jmax - 1);

(*number of computation steps to be run*)

tsteps = 800;

(*calculate "acceleration" factor *)

ω =2/(1 +(1 -((Δz^ 2Cos[π/imax] + Δr^ 2Cos[π/jmax])/(Δz^ 2 + Δr^ 2))^ 2)^ (1/2));

(*calculation variables*)

(*SOR coefficient of f, the poisson eq source term*)

cf = ω/(2(1/Δr^ 2 + 1/Δz^ 2));

(*table of SOR coefficients for the potential at the i + 1 grid point*)

ciplus = Table[cf (1 + 1/(i - .5))/Δ r^ 2, { i, 1,imax }];

(*table of SOR coefficients for the potential at the i - 1 grid point*)

ciminus = Table[cf (1 - 1/(i - .5))/Δr^ 2, { i, 1,imax }];

(*SOR coefficient for potential at the j + 1 and j - 1 grid points*)

cj = cf/Δz^ 2;

(*set up distribution functions for self consistent calculation*)

(* set radial profile of each component*)

α = -2.3 Log[1 - λD/rw];

h[i_] := (1 - ((i/imax)^ α));

qβp = q0 βpos;

qβn = q0 βneg;

dpos[i_, j_] := Exp[qβp(ϕ[[i, 1]] - ϕ[[i,j]])]h[i] ;

(*antishielding distribution*)

dneg[i_, j_] := Exp[qβn(ϕ[[i, j]] - ϕ0)]Erfc[Re[(qβn(ϕ[[i, j]] - ϕ0))^ (1/2)]]h[i];

kpos = q0/ϵ0 n0pos;

kneg = q0/ϵ0 n0neg;

```
(*Poisson eq source term f*)
(*note the If statement cuts off innerwell species in outer well approximately*)
f[i_, j_] :=  If[z1/zw*jmax - j > 0, -kpos dpos[i, j], 0] + kneg dneg[i, j]/dneg[1, 1];
(* Grid setup*)
ϕ  =  Table[0, { i, imax }, { j, jmax }];
(*setup boundary conditions*)
(*the voltages v2 and v4 are set in nested well profile at r = rw for the boundary
condition as well as all other r values as an initial guess for the potential*)
Do[ϕ[[i, j]]  =  v2, { j, Floor[z1/Δz + 1], Floor[z3/Δz + 1] }, { i, 1, imax }];
Do[ϕ[[i, j]]  =  v4, { j, Floor[z3/Δz + 1] + 1, jmax }, { i,1, imax }];
(*set the "end cap" voltage*)
Do[ϕ[[i, jmax]]  =  v4, { i, 1, imax }];
(*empty list to hold residual after each timestep to test convergence*)
reslist = { };
(*the SOR loop*)
Do[res = 0;
   Do[
      Do[
         temp  = ciplus[[i]]ϕ[[i + 1,j]] + ciminus[[i]]ϕ[[i - 1,j]] +
         cj(ϕ[[i,j + 1]] +ϕ[[i,j - 1]]) - cf f[i, j] - ω ϕ[[i,j]];
         res  +=  Abs[temp];
         ϕ[[i, j]]  +=  temp
      , { j, 2, jmmo }]
   ,{ i, 2, immo }];
```

```
    Do[φ[[1, j]]  =  φ[[2,j]], { j, 1, jmax }];
    Do[φ[[i,1]]  =  φ[[i,2]], { i, 1, imax }];
    AppendTo[reslist, res],
{ t, 1, tsteps }]
```

APPENDIX C

ION ORBIT CODE

(*This code calculates single particle trajectories classically for ions in a set of nested electric potential wells with a superimposed constant magnetic field. The potential ϕ which is used has been previously calculated by another program which self - consistently determined the potential and particle distributions within the trap. Given this potential and the magnetic field strength, this code follows the trajectory of individual ions of a given charge state under the effects of both the electric and magnetic forces. The ions are started in the z = 0 plane (the trap's midplane), they are given initial velocities sampled from a Maxwellian velocity distribution (negative z velocities are interpreted as positive due to trap symmetry). The code allows the particle to be tracked as they move through the trap and either make contact with one of the electrode walls or return to the z = 0 plane. The program may also be set to track the particle as it makes several passes through the trap and returns to the z = 0 plane. Statistics are kept on the number of ion escaping (contacting an electrode wall), whether the escaping ions left through a radial or axial wall, and which initial conditions lead to escape and which lead to confinement.*)

(*initialize parameters*)

(*trap parameters*)

(*inner radius of electrode wall*)

rw = .005;

(*1/2 trap length*)

zw = .05;

(*axial magnetic field in T*)

Bz = 10;

```
(*plasma parameters*)
(*charge state of ions*)
cS = 17;
q0 = 1.602*10 ^ -19;
(*β in 1/joules*)
βp = 1/(3000*q0);
(*mass of Ar atom*)
m = 39.9 *1.67*10 ^ -27;
(*computational parameters*)
(*maximum number of timesteps allowed for each particle*)
maxtime = 5000;
(*number of particles*)
maxparticles = 1000;
Δtime = 5*10 ^ -10;(*time per timestep*)
(*In this calculation it is necessary to calculate the rotation of the particle's velocity
vector due to the magnetic field the following Sin and Cos terms are used often in
the loop, so they are given a numerical value now to speed computation.*)
cCos = Cos[-q0 cS Bz/m Δtime];
cSin = Sin[-q0 cS Bz/m Δtime];
(*Set up particle lists The following are empty lists which will be filled with the
initial conditions (x, y, z, vx, vy, vz) of particles which escape radially, escape
axially, and remain confined.*)
esRadvx = {}; esRadvy = {}; esRadvz = {}; esRadx = {}; esRady = {};
esRadz = {};
```

esAxvx = {}; esAxvy = {}; esAxvz = {}; esAxx = {}; esAxy = {}; esAxz = {};

confvx = {}; confvy = {}; confvz = {}; confx = {}; confy = {}; confz = {};

(*The following are empty lists that will store the final positions and velocities of particles that return to the z = 0 plane, so that these values may be used as initial conditions in future runs.*)

finalvx = {}; finalvy = {}; finalvz = {}; finalx = {}; finaly = {}; finalz = {};

(*Load ϕ The list of previously calculated ϕ values.This should be an array of size imax*jmax.*)

ϕ =

imax = Length[ϕ];

jmax = Length[ϕ[[1]]];

(*distance between computation points in r*)

Δr = rw/(imax - 1);

(*distance between computation points in z*)

Δz = zw/(jmax - 1);

immo = imax - 1;

jmmo = jmax - 1;

(*Set up Electric field component tables Set up tables for electric field components in r and z direction.*)

fieldr = Table[0, {i, 1, imax}, {j, 1, jmax}];

fieldz = Table[0, {i, 1, imax}, {j, 1, jmax}];

```
(*Fill in electric field values from φ*)
Do[{fieldr[[i, j]] = φ[[i - 1, j]] - φ[[i + 1, j]]/2Δr,
    fieldz[[i,j]] = φ[[i, j - 1]] - φ[[i, j + 1]]/ 2 Δz}, {i, 2, immo}, {j, 2, jmmo}];
Do[{fieldz[[1,j]] = φ[[1, j - 1]] - φ[[1, j + 1]]/2 Δz,
    fieldz[[imax,j]] = φ[[imax, j - 1]] - φ[[imax, j + 1]]/ 2 Δz}, {j, 2, jmmo}];
Do[{fieldr[[i, 1]] = φ[[i - 1, 1]] - φ[[i + 1, 1]]/2Δr,
    fieldr[[i,jmax]] = φ[[i - 1, jmax]] - φ[[i + 1, jmax]]/ 2Δr}, {i, 2, immo}];
(*Main Program*)
Do[
    (*This section of the code assigns initial conditions. From the initial conditions
chosen, the larmor radius of the particles gyromagnetic motion, rL , is calculated,
as well as the initial location of the center of the particle's orbit*)
    rw = 0;
    rL = 0;
    rc = 0;
    While[rc + rL>=rw,
        posx = Sqrt[Random[]]*rw;
        posy = 0;
        posz = 0;
        posr = posx;
        velperp = Sqrt[-2 Log[Random[]]/(βp m)];
        velx = velperp Cos[θv];
        vely = velperp Sin[θv];
        velz = Abs[Sqrt[2/(βp m)]InverseErf[1 - 2 Random[]]];
```

```
θv = 2π Random[];
initx = posx;
inity = posy
initz = posz;
initvx = velx
initvy = vely
initvz = velz;
rL = m velperp/(q0 cS Bz);
rc = Sqrt[posx ^ 2 + m ^ 2 velperp ^ 2/(Bz cS q0) ^ 2
    - 2 m posx velperp Sin[θv]/Bz cS q0]];
Do[ (*Determine the nearest grid point above and below the ion in both r and
z*)
ipos = Max[{Min[{posr/Δr + 1, imax}], 1}];
jpos = Max[{Min[{posz/Δz + 1, jmax}], 1}];
ilesser = Floor[ipos];
jlesser = Floor[jpos];
igreater = Min[{ilesser + 1, imax}];
jgreater = Min[{jlesser + 1, jmax}];
(*extrapolate from grid values of E - field to value of E - field at the particle's
location*)
efr = (jpos - jlesser)*
    ((ipos - ilesser)*fieldr[[igreater, jgreater]]
    + (ilesser + 1 - ipos)*fieldr[[ilesser, jgreater]])
    + (jlesser + 1 -jpos)*
```

```
        ((ipos - ilesser)*fieldr[[igreater, jlesser]]
        + (ilesser + 1 - ipos)*fieldr[[ilesser, jlesser]]);
    efz =  (jpos - jlesser)*
        ((ipos - ilesser)*fieldz[[igreater, jgreater]]
        + (ilesser + 1 - ipos)*fieldz[[ilesser, jgreater]])
        + (jlesser + 1 - jpos)*
        ((ipos - ilesser)*fieldz[[igreater, jlesser]]
        + (ilesser + 1 - ipos)*fieldz[[ilesser, jlesser]]) ;
(*Convert field in radial coords to cartesian*)
If[posr == 0, {efx = 0, efy = 0} , {efx = posx/posr efr, efy = posy/posr
efr}];
(*update velocities due to electric and magnetic forces*)
tempvx = velx cCos + vely cSin + cS efx Δtime q0/m;
vely = vely cCos - velx cSin + cS q0/m efy Δtime;
velx = tempvx;
velz = q0/m cS efz Δtime + velz;
(*update positions using new velocities*)
posx + = velx Δtime;
posy + = vely Δtime;
posz + = velz Δtime;
posr = Sqrt[posx ^ 2 + posy ^ 2];
AppendTo[poslist, {posx, posy, posz}];
(*Test for particle escape or return to z = 0 and append initial conditions to the
correct list*)
```

```
If[posr > rw, {
    AppendTo[esRadvx, initvx],
    AppendTo[esRadvy, initvy],
    AppendTo[esRadvz, initvz],
    AppendTo[esRadx, initx],
    AppendTo[esRady, inity],
    AppendTo[esRadz, initz],
    Break[]}];
If[posz > zw, {
    AppendTo[esAxvx, initvx],
    AppendTo[esAxvy, initvy],
    AppendTo[esAxvz, initvz],
    AppendTo[esAxx, initx],
    AppendTo[esAxy, inity],
    AppendTo[esAxz, initz],
    Break[]}];
If[ posz < 0, {
    AppendTo[confvx, initvx],
    AppendTo[confvy, initvy],
    AppendTo[confvz, initvz],
    AppendTo[confx, initx],
    AppendTo[confy, inity],
    AppendTo[confz, initz],
    AppendTo[finalvx, velx],
```

```
    AppendTo[finalvy, vely],
    AppendTo[finalvz, velz],
    AppendTo[finalx, posx],
    AppendTo[finaly, posy],
    AppendTo[finalz, posz],
    Break[]}]
, {t, 1, maxtime}]
, {parnum, 1, maxparticles}]
```

BIBLIOGRAPHY

Anderegg, F., E. M. Hollman, and C. F. Driscoll, "Rotating field confinement of pure electron plasmas using Trivelpiece-Gould modes," Phys. Rev. Lett. **81**, 4875 (1998).

Barnes, D. C., T. B. Mitchell, and M. M. Schauer, "Beyond the Brillouin limit with the Penning fusion experiment," Phys. Plasmas **4**, 1745 (1997).

Baur, G., "Production of antihydrogen," Phys. Lett. B **368**, 251 (1996).

Baur, G. et al., "Search for antihydrogen at LEAR," Phys. At. Nuclei **59**, 1509 (1996).

Bluhm, R., V. A. Kostelecky, and N. Russell, "CPT and Lorentz tests in hydrogen and antihydrogen," Phys. Rev. Lett. **82**, 2254 (1999).

Brillouin, L., "A theorem of Larmor and its importance for electrons in magnetic fields," Phys. Rev. **67**, 260 (1945).

Chang, Y., D. D. Dolliver, and C. A. Ordonez, "Analysis of time-dependant effects when operating nested-well plasma traps for achieving antihydrogen recombination," in *Non-Neutral Plasma Physics III*, edited by J. L. Bollinger, R. L. Spencer, and R. C. Davidson (American Institute of Physics, Melville, New York, 1999).

Davidson, R. C., *Physics of Nonneutral Plasmas*, (Addison-Wesley Publishing Company, Redwood City, California, 1990).

Dubin, D. H. and T. M. O'Neil, "Trapped nonneutral plasmas, liquids, and crystals (the thermal equilibrium states)," Reviews of Modern Physics **71**, 87 (1999).

Eades, J. and F. J. Hartmann, "Forty years of antiprotons," Rev. Mod. Phys. **71**, 373 (1999).

Fedichev, P. O., "Formation of antihydrogen atoms in an ultra-cold positron-antiproton plasma," Phys. Lett. A **226**, 289 (1997).

Furth, H. P., "Existence of mirror machines stable against interchange modes," Phys. Rev. Lett. **11**, 308 (1963).

Gabrielse, G. et al., "The ingredients of cold antihydrogen simultaneous confinement of antiprotons and positrons at 4 K," Phys. Lett. B **455**, 311 (1999).

Gabrielse, G., S. l. Rolston, L. Haarsma, and W. Kells, "Antihydrogen production using trapped plasmas," Phys. Lett. A **129**, 38 (1988).

G.Gabrielse et al., "First capture of antiprotons in a Penning trap: A kiloelectronvolt source," Phys. Rev. Lett. **57**, 2504 (1986).

Gilson, E. and J. Fajans, "Quadrupole induced resonant particle transport in a pure electron plasma," in *Non-Neutral Plasma Physics III*, edited by J. L. Bollinger, R. L. Spencer, and R. C. Davidson (American Institute of Physics, Melville, New York, 1999).

Glinsky, M. E. and T. M. O'Neil, "Guiding center atoms: Three body recombination in a strongly magnetized plasma," Phys. Fluids B. **3**, 1279 (1991).

Goldston, R. J. and P. H. Rutherford, *Introduction to Plasma Physics*, (Institute of Physics Publishing, Philadelphia, 1995).

Greaves, R. G. and C. M. Surko, "Antimatter plasmas and antihydrogen," Phys. Plasmas **4**, 1528 (1997).

Greaves, R. G., M. D. Tinkle, and C. M. Surko, "Modes of a pure ion plasma at the Brillouin limit," Phys. Rev. Lett. **74**, 90 (1995).

Hall, D. S. and G. Gabrielse, "Electron cooling of protons in a nested Penning trap," Phys. Rev. Lett. **77**, 1962 (1996).

Hansen, C. and J. Fajans, "Dynamic and Debye shielding and antishielding in magnetized, collisionless plasmas," Phys. Rev. Lett. **74**, 4209 (1995).

Hansen, C., A. B. Reimann, and J. Fajans, "Dynamic and Debye shielding and anti-shielding.," Phys. Plasmas **3**, 1820 (1996).

Haseroth, H. and C. E. Hill, "Multicharged ion sources for pulsed accelerators (invited)," Rev. Sci. Instrum. **67**, 945 (1996).

Holzscheiter, M. H. and M. Charlton, "Ultra-low energy antihydrogen," Rep. Prog. Phys. **62**, 1 (1999).

Kurihara, K., Y. Kiwamoto, T. Saito, K. Yatsu, and S. Miyoshi, "Study of potential formation in an open magnetic field configuration," J. Phys. Soc. Jpn. **61**, 3153 (1992).

Marrs, R. E., S. R. Elliot, and D. A. Knapp, "Production and trapping of hydrogenlike and bare uranium ions in an electron beam ion trap," Phys. Rev. Lett. **72**, 4082 (1994).

McWhirter, W. P., "Spectral intensities," in *Plasma Diagnostic Techniques*, edited by R. H. Huddlestone and S. L. Leonard (Academic Press, New York, 1965), Chap. 5.

Möhl, D., "Production of low-energy antiprotons," Hyperfine Interactions **109**, 33 (1997).

Mitchell, T. B., M. M. Schauer, and D. C. Barnes, "Observation of spherical focus in an electron Penning trap," Phys. Rev. Lett. **78**, 58 (1997).

O'Neil, T. M., "Plasmas with a single sign of charge," in *Non-Neutral Plasma Physics*(American Institute of Physics, New York, 1988).

Ordonez, C. A., "Fully kinetic plasmas-sheath theory for a cold-electron emitting surface," Phys. Fluids B **4**, 778 (1992).

Ordonez, C. A., "Effect of a plasma sheath and ion injection on axial particle and energy confinement in a collisional mirror plasma," Phys. Plasmas **1**, 1359 (1994).

Ordonez, C. A., "Time-dependent nested-well plasma trap," IEEE Trans. on Plasma Sci. **24**, 1378 (1996).

Ordonez, C. A., "Confinement of a neutral plasma using nested electric potential wells," Phys. Plasmas **4**, 2313 (1997).

Ordonez, C. A., "Magnetic cusp and electric nested- or single-well configurations for high density antihydrogen and fusion nonneutral plasma applications," in *Non-Neutral Plasma Physics III*, edited by J. L. Bollinger, R. L. Spencer, and R. C. Davidson (American Institute of Physics, Melville, New York, 1999).

Peurrung, A. J. and J. Fajans, "Non-neutal plasma shapes and edge profiles," Phys. Fluids B **2**, 693 (1990).

Post, R. F., "The magnetic mirror approach to fusion," Nucl. Fusion **27**, 1579 (1987).

Prasad, S. A. and T. M. O'Neil, "Finite length thermal equilibria of a pure electron plasma column," Phys. Fluids **22**, 278 (1979).

Press, W. H., *Numerical Recipes in FORTRAN*, (Cambride University Press, New York., 1992).

Saito, T. et al., "Scaling study of potential in the end region of a tandem mirror based on end-loss electron measurement," Phys. Fluids B **5**, 866 (1993).

Schmidt, G., *Physics of High Temperature Plasmas*, (Academic Press, New York, 1979).

Schwager, L. A., "Effects of secondary and thermionic electron emission on the collector and source sheaths of a finite ion temperature plasma using kinetic theory and numerical simulation," Phys. Fluids B **5**, 631 (1993).

Schwager, L. A. and C. K. Birdsall, "Collector and source sheaths of a finite ion temperature plasma," Phys Fluids B **2**, 1057 (1990).

Spencer, R. L. and G. W. Hart, "Linear theory of non-neutral plasma equilibrium in a tilted magnetic field," Phys. Fluids B **4**, 3507 (1992).

Spencer, R. L., S. N. Rasband, and R. R. Vanfleet, "Numerical calculation of axisymmetric non-neutral plasma equilibria," Phys. Fluids B **5**, 4267 (1993).

Tatematsu, Y., Y. Kiwamoto, T. Saito, and T. Tamano, "Effects of Yushmanov-trapped particles and anisotropy of velocity distribution on the potential formation in the end region of the tandem mirror," J. Phys. Soc. Jpn. **63**, 558 (1994).

Tatematsu, Y. et al., "Control of plasma transport by active tailoring of potential profile along open magnetic fields," J. Nucl. Mater **220-222**, 575 (1995).